Chapter 4

Solution of Integral Equations for Wire Radiators and Scatterers

4.1 Formulation

Let us consider a wire of length 2ℓ and radius a ($\ell \gg a$), as shown in Fig. 4.14.1. The wire is excited by an incident field $\mathbf{E}^i$ and we are interested in computing the current generated on the wire due to this excitation. Upon determination of the current we can then compute the radiated field in the usual manner.

To solve for the wire surface currents, we must enforce the boundary condition demanding that the total tangential electric field vanishes on the surface of the perfectly conducting wire. That is,

$$E_z^{tot} = E_z^i + E_z^r = 0 \tag{4.1}$$

where E_z^r is the field radiated by the wire surface current density $\mathbf{J}(\phi, z) = \hat{z}J_z(\phi, z) + \hat{\phi}J_\phi(\phi, z)$. However, on the assumption of a very thin wire, i.e. $k_oa \ll 1$, where $k_o = 2\pi/\lambda_o$ is the free space wavenumber, $J_\phi(\phi, z)$ will either be negligible or not effect the radiated field. Thus, from (2.52a2.52a), (2.109c 2.109c) or (2.102a 2.102a) in conjunction with (2.101 2.101) we may express the ~~wire~~ radiated field as

$$\mathbf{E}^r(\rho, \phi, z) = -jk_oZ_o\hat{z}\int_{-\ell}^{\ell}\int_0^{2\pi} J_z(\phi', z')\left(1 + \frac{1}{k_o^2}\frac{\partial^2}{\partial z^2}\right)\frac{e^{-jk_oR}}{4\pi R}\, a\, d\phi'\, dz' \tag{4.2}$$

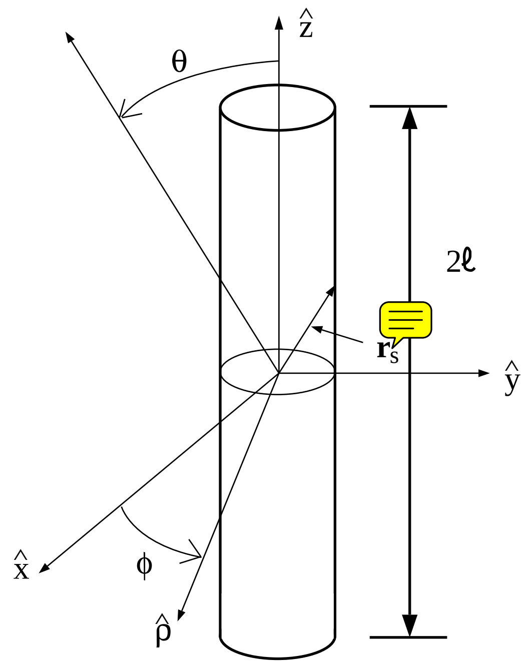

Figure 4.1: Cylindrical wire geometry.

in which $Z_o = 1/Y_o$ denotes the free space intrinsic impedance and

$$R = |\mathbf{r} - \mathbf{r}'| = \sqrt{\rho^2 + a^2 - 2\rho a \cos(\phi - \phi') + (z - z')^2} \tag{4.3}$$

since $\mathbf{r} = \rho\hat{\rho} + z\hat{z}$ and $\mathbf{r}' = a\hat{\rho} + z'\hat{z}$. This expression can be further simplified by assuming that $J_z(\phi, z)$ is symmetric with respect to ϕ, a reasonable assumption since the wire is very thin and is typically part of a transmission line fed by a voltage source at its center. The surface current $J_z(\phi, z)$ can then be equivalently replaced by a filamentary line current $I(z)$ placed at the center of the tubular conductor. For the two currents to generate the same field when $\rho \gg a$, it is necessary that they satisfy the relation

$$I(z) = \int_0^{2\pi} J_z(\phi, z) a d\phi = 2\pi a J_z(z). \tag{4.4}$$

Introducing this into (4.2 4.2) yields

$$E_z^r(\rho, \phi = 0, z) = E_z^r(\rho, z) = -jk_o Z_o \int_{-\ell}^{\ell} I(z') \left(1 + \frac{1}{k_o^2} \frac{d^2}{dz^2}\right) G_w(z - z') dz' \tag{4.5}$$

where

$$G_w(z - z') = \frac{1}{2\pi} \int_0^{2\pi} \frac{e^{-jk_o\sqrt{\rho^2 + a^2 - 2\rho a \cos\phi' + (z - z')^2}}}{4\pi\sqrt{\rho^2 + a^2 - 2\rho a \cos\phi' + (z - z')^2}} d\phi' \tag{4.6}$$

and we have arbitrarily set $\phi = 0$ since by symmetry the radiated field is expected to be independent of ϕ.

To construct the integral equation for the solution of the current $I(z)$ we set $\rho = a$ in (4.6 4.6) and substitute (4.5 4.5) into (4.1 4.1). This gives

$$E_z^i(\rho = a, z) = +jk_o Z_o \int_{-\ell}^{\ell} I(z') \left(1 + \frac{1}{k_o^2} \frac{d^2}{dz^2}\right) G_{wu}(z - z') dz' \tag{4.7}$$

The kernel $G_{wu}(z - z')$ is now given by

$$G_{wu}(z - z') = \frac{1}{2\pi} \int_0^{2\pi} \frac{e^{-jk_o R_u}}{4\pi R_u} d\phi' \tag{4.8}$$

with

$$R_u = \sqrt{(z - z')^2 + 4a^2 \sin^2(\phi'/2)} \tag{4.9}$$

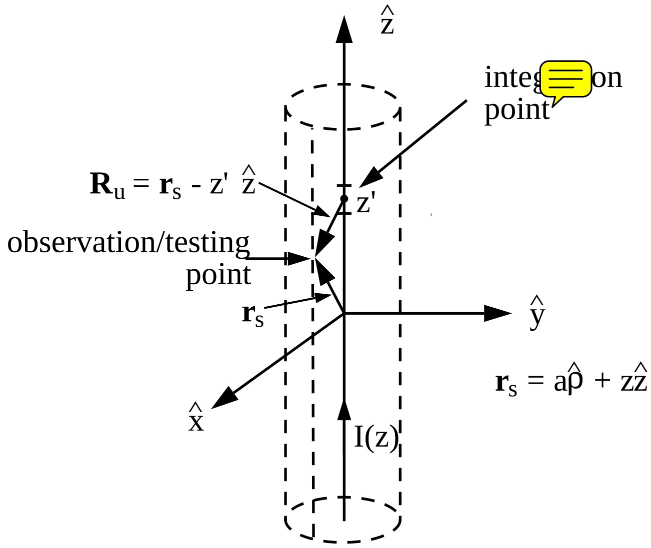

Figure 4.2: Geometry for testing on the wire surface.

G_{wu} is often referred to as the unreduced thin wire kernel. In practice, though, to avoid the integration over ϕ', $G_{wu}(z - z')$ is replaced by the reduced kernel

$$G_{wr}(z - z') = \frac{e^{-jk_o\sqrt{(z-z')^2+a^2}}}{4\pi\sqrt{(z - z')^2 + a^2}} = \frac{e^{-jk_oR_o}}{4\pi R_o} \tag{4.10}$$

which is obtained by letting $\mathbf{r}' = z'\hat{z}$. That is, the reduced kernel refers to the problem where the filamentary current is introduced from the start of the analysis. Substituting (4.10 4.10) into the integral equation (4.74.7) gives

$$E_z^i(\rho = a, z) = jk_oZ_o \int_{-\ell}^{\ell} I(z') \left(1 + \frac{1}{k_o^2}\frac{d^2}{dz^2}\right) \frac{e^{-jk_oR_o}}{4\pi R_o} dz' \tag{4.11}$$

with R_o as defined in (4.104.10). One readily observes that the right hand side of this equations is simply the negative of the field radiated by the filamentary current $I(z)$ and evaluated at $\rho = a$, (i.e. on the surface of the perfectly conducting wire as shown in Fig. 4.24.2. Obviously, (4.114.11) could have been derived in a more direct manner by first invoking the approximation (4.44.4) and then referring to the integral representation (2.109c2.109c). Nevertheless, the above steps should serve to clarify the implied approximations. As will be shown later, (4.74.7) and (4.114.11) can be solved with nearly equal efforts when an iterative solution scheme is employed.

The thin wire integral equation (4.114.11) is commonly referred to as Pocklington's integral equation [?][Pocklington, 1897]. More generally, it belongs to the general class of Fredholm integral equations of the first kind. These are characterized by the presence of the unknown function only under the integral whose limits are constant. Integral equations which have the unknown quantity both under and outside the integral are of the second kind and we shall consider them at the end of this chapter. Also, if the integral limits are not constant, then the corresponding integral equations are of the Voltera type which are the typical equations for non-harmonic (time-dependent) field quantities.

An analytical solution of (4.114.11) is not possible unless the wire is semi-infinite in which case function theoretic techniques such as the Weiner-Hopf method [?][Noble, 1958] can be employed for its solution in the transform domain. However, Pocklington's integral equation can be numerically solved without difficulty, particularly because the integral's kernel is never singular since $R_o > a$ for all values of z and z'. Nevertheless, to reduce the kernel's singularity, it is still instructive to transfer one of the derivatives from the Green's function to the current as was done in section 3.1.2 in conjunction with the Stratton-Chu integral equation. In particular, from the one-dimensional form of (3.123.12) via integration by parts we have (note $\frac{d}{dz}G_{wr} = -\frac{d}{dz'}G_{wr}$)

$$\int_{-\ell}^{\ell} I(z')\frac{d^2}{dz^2}G_{wr}(z-z')dz' = \int_{-\ell}^{\ell} \frac{dI(z')}{dz'}\,\frac{d}{dz}G_{wr}(z-z')dz' - \frac{d}{dz}\left[G_{wr}(z-z')I(z')\right]_{z'=-\ell}^{z'=\ell} \tag{4.12}$$

Since the current at the wire ends must vanish, we observe that the last term of (4.124.12) is zero and thus Pocklington's integral equation can be rewritten as

$$E_z^i(\rho = a, z) = jk_oZ_o\int_{-\ell}^{\ell}\left[I(z')G_{wr}(z-z') + \frac{1}{k_o^2}\,\frac{d}{dz'}I(z')\frac{d}{dz}G_{wr}(z-z')\right]dz' \tag{4.13}$$

An alternative way to derive Pocklington's equation is through the use of the vector and scalar potentials. Accordingly, from (2.42.4) E_z^r can be expressed as

$$E_z^r(\rho, z) = -jk_o Z_o A_z - \frac{\partial \Phi_e}{\partial z} \tag{4.14}$$

where

$$A_z(\rho = a, z) = \int_{-\ell}^{\ell} I(z') \frac{e^{-jk_o R_o}}{4\pi R_o} dz' \tag{4.15}$$

and

$$\Phi_e(\rho = a, z) = \int_{-\ell}^{\ell} \frac{\rho(z')}{\epsilon_o} \frac{e^{-jk_o R_o}}{4\pi R_o} dz' \tag{4.16}$$

From the continuity equation (1.331.33) we have

$$\frac{\rho(z)}{\epsilon_o} = -\frac{Z_o}{jk_o} \frac{dI(z)}{dz} \tag{4.17}$$

and, thus, when (4.144.14) along with (4.154.15) – (4.174.17) is substituted into (4.14.1) we obtain (4.134.13).

The standard procedure for solving the above integral equation amounts to first expanding the currents in terms of a class of basis functions. That is, $I(z)$ is approximately expressed as a linear sum of N known expansion functions. Upon substitution of this expansion into (4.134.13) we obtain an equation for the coefficients of the expansion which is a function of the surface observation point z. The second step in the numerical solution process is the enforcement of the integral equation at specific values of z. In this manner we obtain a single linear equation for each enforcement point. If we have N expansion coefficients, a total of N linear equations must then be generated by changing the location of the testing point. These comprise a system which can be solved for the unknown expansion coefficients. Depending on the type of expansion functions or enforcement scheme, different linear systems will be obtained. The procedure of expanding the current in terms of a finite set of functions and then enforcing the boundary condition is referred to as the discretization of the integral equation. Discretization is therefore the procedure which generates the linear system. In turn, the resulting system can be solved through various direct or iterative methods to obtain the coefficients of the expansion. A knowledge of these provides an approximation for the current distribution and once the current is known we can proceed with the computation of the radiated field, input impedance, radiated power and gain of the antenna using standard formulae.

Before proceeding with the discretization of the integral equation (4.114.11) as discussed above, we first present some of the most commonly used expansion basis for the current distributions.

4.2 Basis Functions

A first step in discretizing (4.94.9) is to expand the current distribution as

$$I(z) = \sum_{n=0}^{N-1} I_n f_n(z) = \sum_{n=0}^{N-1} I_n f(z - z_n) \tag{4.18}$$

where $f_n(z)$ are the basis functions of the expansion and I_n are unknown expansion coefficients. Referring to Fig. 4.34.3, some of the most popular choices for $f_n(z)$ are

(1) Pulse basis functions/Piecewise constant (PWC):

$$f_n(x) = P_{\Delta x}(x - x_n) = \begin{cases} 1 & x_n - \frac{\Delta x}{2} < x < x_n + \frac{\Delta x}{2} \\ 0 & \text{elsewhere} \end{cases} \tag{4.19}$$

(2) Triangular function/Piecewise linear:

$$f_n(x) = T_n(x) = \left(1 - \frac{|x - x_n|}{\Delta x}\right) P_{2\Delta x}(x - x_n) \tag{4.20}$$

(3) Piecewise sinusoidal (PWS):

$$f_n(x) = S_n(x) = \frac{\sin k_o(\Delta x - |x - x_n|)}{\sin k_o \Delta x} P_{2\Delta x}(x - x_n) \tag{4.21}$$

where Δx is usually small (of the order $\lambda_o/10$) and $N = 2\ell/\Delta x$. Because their domain is confined to a small section of the wire, they are commonly referred to as subsectional or subdomain basis functions. A major reason for their popularity is owed to their capability to model any arbitrary function provided Δx is sufficiently small.

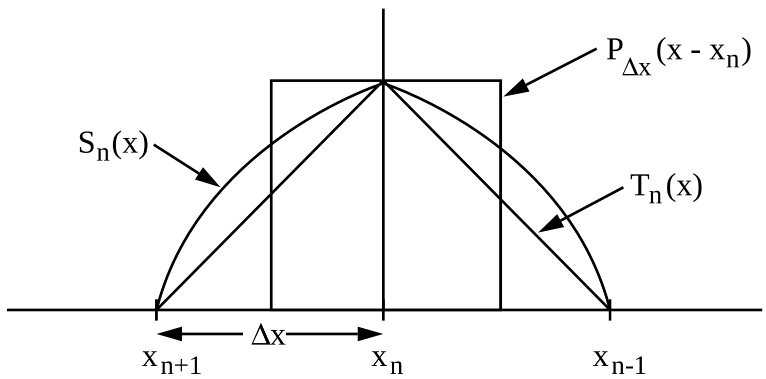

Figure 4.3: Three subsectional expansion functions.

As illustrated though in Fig. 4.44.4, they cause artificial discontinuities in the current or its derivatives at the transition between two consecutive expansion functions. Specifically, the current expansion with the PWC basis is inherently discontinuous at the junction of two adjacent segments and from (4.174.17) this implies the existence of a fictitious charge at that point. Nevertheless, in spite of this deficiency when the segments are sufficiently small, they provide a reasonable approximation to the current distribution. In that case, the constant value over the segment should be interpreted to represent the average of the true current over that segment. Because of their simplicity, and this will soon be apparent in the next section, they have been used extensively in electromagnetics but more so for scattering than antenna parameter computations. In the last case, excessive sampling may be required for the correct evaluation of the antenna's input impedance.

The piecewise linear basis are seen to generate continuous current distributions. This is because the adjacent basis are overlaid as shown in Fig. 4.4(b)4.4(b). Thus, the current at any point on the wire is obtained by summing the overlaid basis. From their definition, though, when one of the overlaying expansion functions is at a maximum, the left and right adjacent expansion functions are zero. Further, because each expansion is normalized, the coefficients correspond to the current's value at the middle of the nth segment. The PWS expansion functions are very similar to the linear basis in nearly all respects. One difference between the two is that the PWS basis can be differentiated any arbitrary number of times within its range without vanishing. Nevertheless, similarly to the piecewise linear basis they also yield a current expansion

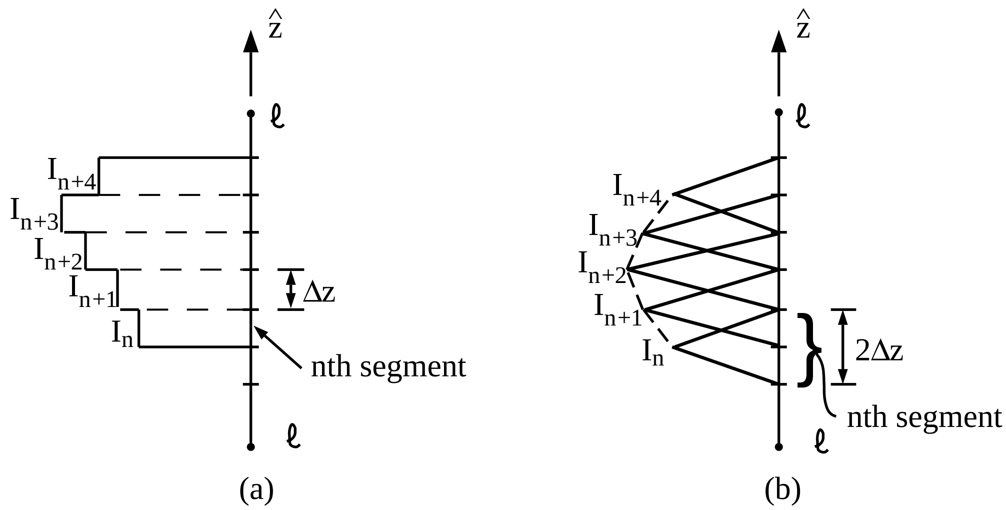

Figure 4.4: Illustration of wire segmentation and current approximation with subdomain basis (a) pulse basis expansion (b) triangular basis expansion.

that has a discontinuous first derivative at the middle of each wire segment. The only advantage of the PWS basis is drawn from their property to yield potential integrals which can be evaluated analytically once $S_n(x)$ is expressed as a sum of two exponentials.

Instead of using the above subsectional or subdomain basis to represent the wire current one could alternatively employ the usual full basis expansions such as $\cos nx$ and $\sin nx$. For example, noting that $I(\pm\ell) = 0$, an appropriate expansion for the wire current would be

$$I(z) = \sum_{n=1}^{N} C_n \cos\left[\frac{(2n-1)\pi z}{2\ell}\right] \tag{4.22}$$

or

$$I(z) = \sum_{n=1}^{N} C_n \sin\left[\frac{(2n-1)\pi z}{\ell}\right] \tag{4.23}$$

In contrast to the expansions (4.194.19) – (4.214.21), the coefficients of these expansions do not coincide with specific values of the current $I(z)$. More importantly, N may have to be quite large in case $I(z)$ is rapidly varying or not sinusoidal in form. However, for wire antennas $I(z)$ is generally sinusoidal, particularly when the wire is excited by an external incident field. In this case only a few terms of the full basis expansions (4.224.22) or (4.234.23) may be required, making them attractive. Generally, though, (4.224.22) – (4.234.23) cannot be effectively used for curved wires or other complex wire structures on which the current's distribution is much more irregular. In the following, we shall therefore concentrate on the discretization and solution of Pocklington's integral equation using subdomain/basis functions since such a solution is less specific to the straight wire.

4.3 Pulse Basis–Point Matching Solution

For simplicity, let us first consider the pulse basis expansion to represent the wire current distribution. This results in a summation of shifted pulses over the total length of the wire, i.e.

$$I(z) = \sum_{n=0}^{N-1} I_n P_{\Delta z}(z - z_n) \tag{4.24}$$

where

$$N = \frac{2\ell}{\Delta z} \tag{4.25}$$

are the number of pulses used to approximate the current distribution on the wire and

$$z_n = -\ell + \left(n - \frac{1}{2}\right)\Delta z; \quad n = 0, 1, 2, \ldots \tag{4.26}$$

Substituting (4.244.24) into (4.134.13) yields

$$E_z^i = \frac{jk_o Z_o}{4\pi}\left\{\sum_{n=0}^{N-1} I_n \int_{z_n-\frac{\Delta z}{2}}^{z_n+\frac{\Delta z}{2}} \frac{e^{-jk_o R_o}}{R_o} dz' + \frac{1}{k_o^2}\sum_{n=0}^{N-1} I_n \frac{d}{dz} \cdot \left[\frac{e^{-jk_o R_{1n}}}{R_{1n}} - \frac{e^{-jk_o R_{2n}}}{R_{2n}}\right]\right\} \tag{4.27}$$

where

$$R_{1n} = \sqrt{\left(z - z_n + \frac{\Delta z}{2}\right)^2 + a^2}\,, \qquad R_{2n} = \sqrt{\left(z - z_n - \frac{\Delta z}{2}\right)^2 + a^2} \quad (4.28)$$

and we have invoked the expression

$$\frac{dI(z)}{dz} = \sum_{n=-N/2}^{N/2} I_n \left[\delta\left(z - z_n + \frac{\Delta z}{2}\right) - \delta\left(z - z_n - \frac{\Delta z}{z}\right)\right] \quad (4.29)$$

in deriving (4.274.27). After differentiating the last term of (4.274.27) with respect to z, we obtain

$$E_z^i(\rho = a, z) = \frac{jZ_o}{2\lambda_o} \sum_{n=0}^{N-1} I_n \left[\Psi_n(z) + \Phi_n(z)\right] \quad (4.30)$$

where

$$\Psi_n(z) = \int_{z_n - \frac{\Delta z}{2}}^{z_n + \frac{\Delta z}{2}} \frac{e^{-jk_o R_o}}{R_o} dz' \quad (4.31)$$

and

$$\begin{aligned} \Phi_n(z) = -k_o \Bigg[& \left(z - z_n + \frac{\Delta z}{2}\right) \frac{(jkR_{1n} + 1)}{(k_o R_{1n})^3} e^{-jk_o R_{1n}} \\ & - \left(z - z_n - \frac{\Delta z}{2}\right) (jk_o R_{2n} + 1) \frac{e^{-jk_o R_{2n}}}{(k_o R_{2n})^3} \Bigg] \end{aligned} \quad (4.32)$$

Equation (4.304.30) can now be solved for I_n by demanding that it be satisfied (matched) at N points on the surface of the wire. A convenient set of such points is

$$z = z_m = -\ell + \left(m - \frac{1}{2}\right)\Delta z, \quad m = 0, 1, 2, 3, \ \ldots$$

with $\phi = 0$, i.e. along the line formed by the wire surface and the xz plane.

This results in a set of matrix equations

$$\begin{bmatrix} Z_{00} & Z_{01} & Z_{02} & \cdots & Z_{0n} & \cdots & Z_{0,N-1} \\ Z_{10} & Z_{11} & Z_{12} & \cdots & Z_{1n} & \cdots & Z_{1,N-1} \\ \vdots & & \vdots & & \vdots & & \vdots \\ Z_{m0} & Z_{m1} & Z_{m2} & \cdots & Z_{mn} & \cdots & Z_{m,N-1} \\ \vdots & & \vdots & & \vdots & & \vdots \\ Z_{(N-1),0} & Z_{(N-1),1} & Z_{(N-1),2} & \cdots & Z_{(N-1),n} & \cdots & Z_{(N-1),(N-1)} \end{bmatrix} \begin{bmatrix} I_o \\ I_1 \\ I_2 \\ \vdots \\ I_m \\ \vdots \\ I_{N-1} \end{bmatrix}$$

$$= \begin{bmatrix} V_1 \\ V_2 \\ V_3 \\ \vdots \\ V_m \\ \vdots \\ V_{N-1} \end{bmatrix}$$

which are commonly written as

$$[Z_{mn}]\{I_n\} = \{V_m\} \tag{4.33}$$

Obviously,

$$\{I_n\} = \left\{I_0, I_1, I_2, \ldots, I_{N/2}, \ldots, I_{N-1}\right\}^T \tag{4.34}$$

is a column matrix, $[Z_{mn}]$ is a square matrix referred to as the impedance matrix since in this case the excitation column $\{V_m\}$, where

$$V_m = -E_z^i(\rho = a, z_m) \tag{4.35}$$

has units of volts. The corresponding elements of the impedance matrix can be obtained directly from (4.304.30) – (4.324.32). We find that

$$Z_{mn} = -\frac{jZ_o}{2\lambda_o}\left[\Psi_n(z_m) + \Phi_n(z_m)\right] \tag{4.36}$$

where $\Psi_n(z_m)$ can be rewritten as

$$\Psi_n(z_m) = \int_{(z_m - z_n) - \frac{\Delta z}{2}}^{(z_m - z_n) + \frac{\Delta z}{2}} \frac{e^{-jk_o\sqrt{t^2+a^2}}}{\sqrt{t^2 + a^2}} dt.$$

It is seen that $Z_{nm} = Z_{mn}$, indicating that the impedance matrix is symmetric. It is also observed that $[Z_{mn}]$ is completely independent of the excitation.

The integral $\Psi_n(z_m)$ cannot be evaluated analytically but can be approximated in closed form with sufficient accuracy. For $m \neq n$, $\sqrt{t^2+a^2}$ is not very small and we may therefore employ midpoint integration to approximately express it as

$$\Psi_n(z_m) \approx \Delta z \frac{e^{-jk_o\sqrt{(z_m-z_n)^2+a^2}}}{\sqrt{(z_m-z_n)^2+a^2}}; \quad m \neq 0$$

When $m = n$, $\sqrt{t^2+a^2}$ is nearly zero over the midrange of integration. In this case we can employ the two term expansion

$$e^{-jk_oR} \cong 1 - jk_oR$$

allowing us to approximate $\Psi_n(z_n)$ as

$$\Psi_n(z_n) \approx \int_{\frac{-\Delta z}{2}}^{\frac{\Delta z}{2}} \left[\frac{1}{\sqrt{t^2+a^2}} - jk_o\right] dt = \ln\left(\frac{\sqrt{\left(\frac{\Delta z}{2}\right)^2+a^2}+\frac{\Delta z}{2}}{\sqrt{\left(\frac{\Delta z}{2}\right)^2+a^2}-\frac{\Delta z}{2}}\right) - jk_o\Delta z$$

and for $\Delta z \gg a$ this can be further simplified to give

$$\Psi_n(z_n) \approx 2\ln\left(\frac{\Delta z}{a}\right) - jk_o\Delta z; \quad \Delta z \gg a.$$

An alternative way for computing the integral $\Psi_n(z_m)$ is to *regularize* its near singular integrand with the addition and subtraction of the term $\frac{1}{\sqrt{t^2+a^2}}$ which can be integrated analytically. This gives

$$\begin{aligned}\Psi_n(z_m) &= \int_{(z_m-z_n)-\frac{\Delta z}{2}}^{(z_m-z_n)+\frac{\Delta z}{2}} \left[\frac{e^{-jk_o\sqrt{t^2+a^2}}}{\sqrt{t^2+a^2}} - \frac{1}{\sqrt{t^2+a^2}}\right] dt \\ &+ \ln\left(\frac{\sqrt{\left(z_m - z_n+\frac{\Delta z}{2}\right)^2+a^2}+z_m-z_n+\frac{\Delta z}{2}}{\sqrt{\left(z_m-z_n-\frac{\Delta z}{2}\right)^2+a^2}+z_m-z_n-\frac{\Delta z}{2}}\right)\end{aligned}$$

The new integrand is now slowly varying and can thus be evaluated numerically without difficulty.

To compute the current coefficients we must solve the system (4.334.33) and there are a number of commercially available routines which can perform this operation in a manner transparent to the user. Commonly used software libraries such as IMSL, LINPACK, and NAG include a variety of subroutines for a solution of (4.334.33). These are based on solution methods such as Gauss-Jordan elimination, Gaussian elimination, Crout or LU decomposition, most of which are discussed in numerical analysis textbooks.

If we choose to solve $\{I_m\}$ by inverting the matrix $[Z_{mn}]$, the required CPU time will be approximately

$$t \approx AN^2 + BN^3 + CN^2 N_i \tag{4.37}$$

where N, of course, denotes the number of unknowns or the length of the column $\{I_n\}$ and N_i is the number of different excitations for which $\{I_n\}$ must be computed. In addition,

$$\begin{aligned} A &= \text{time required to compute each value of } Z_{mn} \\ BN^3 &= \text{time required to invert } [Z_{mn}] \end{aligned}$$

and

$$\begin{aligned} CN^2 = {} & \text{time required to perform the matrix} \\ & \text{multiplication } [Z_{mn}]^{-1}\{V_m\}. \end{aligned}$$

The actual values of the constants A, B and C are machine dependent. Expression (4.374.37) holds regardless of the procedure used to obtain the inverse, but clearly, for large N the second term of (4.374.37) dominates. However, a solution for $\{I_n\}$ can be obtained without a need to complete the inverse. In this case the Gauss-Jordan elimination requires N^3 ($\frac{N^2}{2}$ if the inverse is not returned) operations to complete the solution whereas the Gaussian elimination needs $5N^3/6$ operations. In contrast, the LU (Lower-Upper) decomposition approach requires $N^3/3$ operations and is thus much faster. The LU decomposition scheme is also preferred because it results in better accuracy and stability as compared to other methods, particularly when N is large. Nevertheless, when N becomes very large, a direct solution of the linear system (4.334.33) may yield an inaccurate result due to machine round-off errors. An alternative in this case is to use an iterative solution scheme allowing some control on the solution error, and such a scheme is discussed at the end of this chapter.

Often, as is the case with the linear wire discussed here, the impedance matrix will posses certain symmetries which can be exploited in the solution

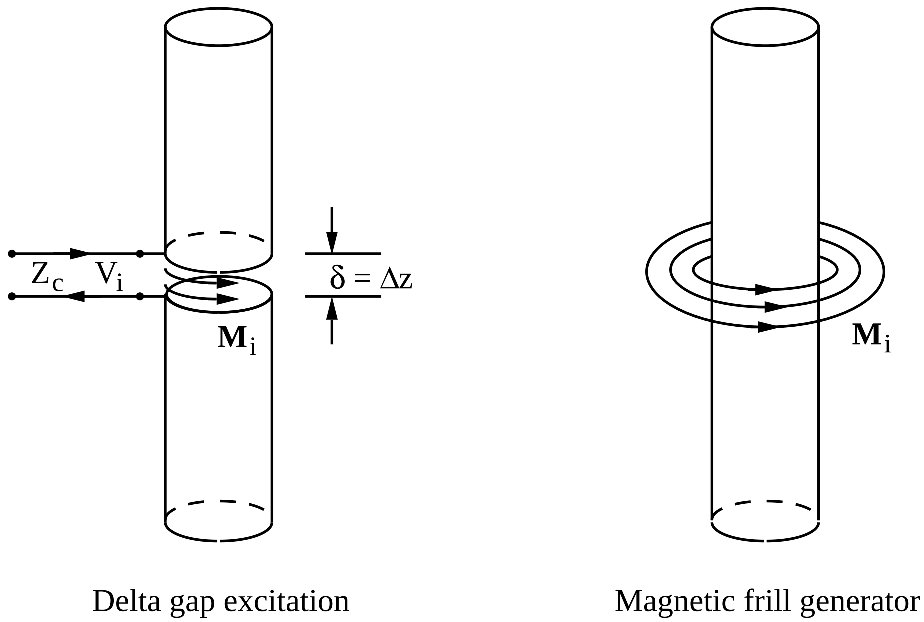

Figure 4.5: Source modeling for the center fed cylindrical dipole.

of (4.334.33). It is easy to observe from (4.284.28), (4.314.31), (4.324.32) and (4.364.36) that $Z_{nm} = Z_{mn} = Z_{m-n} = Z_{|m-n|}$. Matrices of this type are referred to as symmetric Toeplitz and require order N^2 operations to complete the solution. Also, since the elements of $[Z_{mn}]$ can be generated from those in one row or a column, the fill time of the matrix can be reduced to only order N operations. Note, that if we were to consider a solution of the currents on a curved wire, then $Z_{mn} \neq Z_{|m-n|}$ but $Z_{nm} = Z_{mn}$ as a consequence of reciprocity (i.e. the matrix is still symmetric).

4.4 Source Modeling

4.4.1 Delta gap excitation

The wire antenna is usually center fed by a transmission line whose voltage can be measured at the terminals of the antenna. Assuming, the transmission line voltage at the wire terminals is V_i (see Fig. 4.54.5), we may then write [?][Collin, 1985]

$$V_i = -\int_{-\delta/2}^{\delta/2} \mathbf{E}^r \cdot \hat{z} dz = +\int_{-\delta/2}^{\delta/2} E_z^i dz = +E_z^i \delta \tag{4.38}$$

from small δ. Consequently

$$E_z^i = \begin{cases} \frac{+V_i}{\delta} & z = 0 \\ 0 & \text{elsewhere} \end{cases} \tag{4.39}$$

and this is referred to as the delta gap excitation model for the source field E_z^i. Note that (4.394.39) is equivalent to having a magnetic current loop

$$\mathbf{M}^i = -\hat{\rho} \times \mathbf{E}^i = \hat{\phi}\frac{V_i}{\delta} \tag{4.40}$$

of radius a as the excitation. In fact, the derivation of (4.384.38) requires that the delta gap is first closed making the conductor continuous. The excitation field E_z^i which is confined over the original gap length can then be replaced by the equivalent magnetic current loop $\mathbf{M}^i$. This, in turn generates a scattered field E_z^r at the conductor's surface so that the total field $E_z^i + E_z^r$ vanishes as required, a condition which was imposed in deriving (4.384.38). Inherently, the presence of the magnetic current generates discontinuous electric fields across its surface and for this particular case the electric field is zero in the interior side of $\mathbf{M}_i$ and equal to $\hat{z}E_z^i$ at its exterior side.

Wire current distributions obtained by solving the system (4.334.33) in conjunction with a delta gap modeling of the source are illustrated in Figs. 4.64.6 and 4.7 4.7. The curves in each figure correspond to $\lambda_o/2$ and λ_o long dipoles, respectively, of radius $a = 0.005\lambda_o$. It is seen that a rather large number of pulse basis are required for the current to converge to its final value. Generally, (i.e. provided the system has acceptable condition number), the correct distribution is obtained if the computed values of $I(z)$ do not change appreciably as N is increased. Having the correct value of $I(z)$ is extremely important for input impedance computations but the radiation pattern can be predicted with sufficient accuracy once $I(z)$ is known approximately. As expected, the computed current is sinusoidal in form except near the feed point and, thus, it is not surprising that the often assumed sinusoidal behavior of the wire current is sufficient for pattern prediction but much less so for input impedance computations. This is more apparent for the λ_o long dipole in which case the sinusoidal distribution will predict zero current at the feed.

Perhaps one of the reasons for the large number of expansion pulses required to reach convergence is the difficulty of the point matching procedure in satisfying the boundary condition at all z. As seen from Fig. 4.84.8, the wire surface fields obtained by integrating the numerically computed current given in Fig. 4.64.6 do not vanish except at the match points z_m. Nevertheless, on the average, the surface field is zero as can be attested from the oscillatory behavior of the computed surface field given in Fig. 4.84.8. Later, it will be discussed that higher order expansion functions and more robust testing procedures yield more satisfactory results with less unknowns.

In implementing (4.334.33) we were careful to maintain $\frac{\Delta z}{a}$ layer in accordance with the thin wire approximation. Studies [?][Burke and Poggio, 1981] have shown that the thin wire approximation is less than 1% in error if $\frac{\Delta z}{a} < 8$. Since typically $\Delta z \leq \frac{\lambda_o}{10}$, this implies that $k_o a \leq 0.08$ to limit the error to 1%.

4.4.2 Magnetic frill generator

As can be expected, (4.394.39) is not as accurate (particularly as the wire radius becomes greater than 0.007λ [?][Imbriale and Ingerson, AP-T, 1973]) since the field is unlikely to be concentrated only within the gap. An alternative source model giving a smoothly varying excitation field around the gap is the magnetic frill generator. In this case the gap is equivalently replaced by a circumferentially directed surface magnetic current density existing in the region between $\rho = a$ and $\rho = b$, as shown. The value of the outer radius b is computed from a knowledge of the transmission lines characteristic impedance Z_c. When the wire antenna is fed by a coaxial cable it is shown below that the equivalent magnetic frill current can be computed in terms of the aperture fields in the usual manner.

Using the equivalence principle, the aperture is closed and replaced by the surface magnetic current

$$\mathbf{M}^i = \mathbf{E}^a \times \hat{z} \tag{4.41}$$

where

$$\mathbf{E}^a(\rho) = \hat{\rho}\frac{V_i}{2\rho \ln b/a} \qquad (V_i \text{ is a constant}) \tag{4.42}$$

as dictated by the lowest order mode supported in the coaxial transmission line. The radiated field by $\mathbf{M}^i$ may now be evaluated after invoking image

Figure 4.6: Computed current on a center-fed $\lambda_o/2$ dipole of radius $a = .005\lambda_o$ via the pulse basis-point matching solution method as a function of the sampling density. The source/excitation is a delta gap as given in (4.394.39).

Figure 4.7: Computed current on a center-fed λ_o dipole of radius $a = .005\lambda_o$ via the pulse basis-point matching solution method as a function of the sampling density. The source/excitation is a delta gap as given in (4.394.39).

Figure 4.8: Value of the total field on the surface of the dipole computed by integrating the current obtained from a pulse basis-point matching solution ($2\ell = 0.5\lambda$, $a = 0.005\lambda$ and $N = 81$). A value of 5V/m corresponds to a 3.1% error.

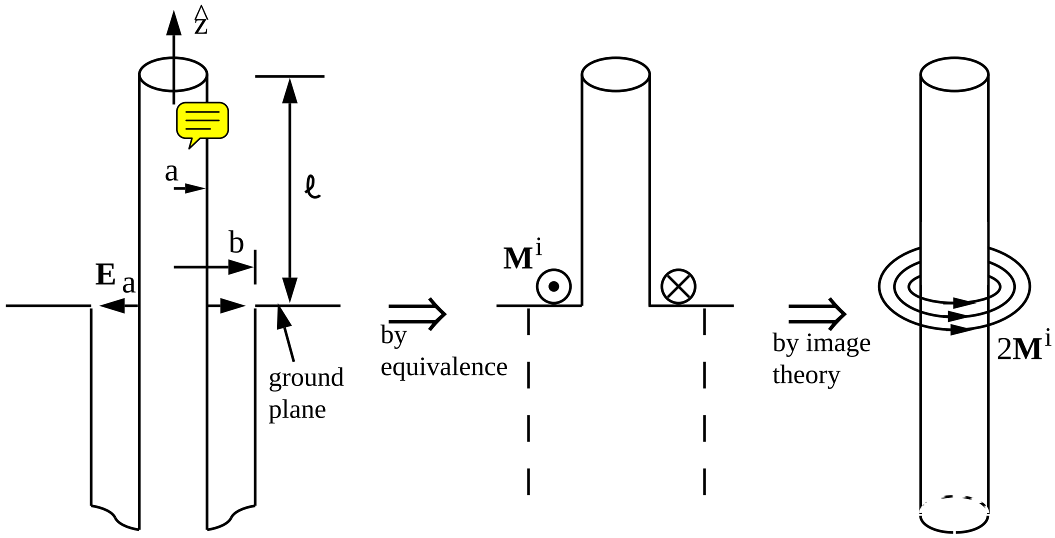

Figure 4.9: Magnetic frill model for a coaxially fed monopole/dipole.

theory to double its strength and the length of the monopole to that of a dipole. From (2.632.63)

$$\mathbf{E}^i(\rho, z) = -\int_a^b \int_0^{2\pi} \left[\mathbf{M}^i(\rho') \times \hat{R}\right] \left(jk_o + \frac{1}{R}\right) \frac{e^{-jkR}}{4\pi R} \rho' d\phi' d\rho' \qquad (4.43)$$

where

$$\mathbf{R} = |\mathbf{r} - \mathbf{r}'|$$

$$\mathbf{r} = \rho\hat{\rho} + z\hat{z}, \qquad \mathbf{r}' = \rho'\hat{\rho} = \rho'(\hat{x}\cos\phi' + \hat{y}\sin\phi')$$

For $\rho = 0$ (observation at the center of the wire)

$$R = \sqrt{(\rho')^2 + z^2}$$

$$\hat{R} = \frac{\mathbf{r} - \mathbf{r}'}{R} = \left[-\hat{\rho}'\rho' + z\hat{z}\right]/R$$

$$\mathbf{M}^i(\rho') = -\hat{\phi}' \frac{V_i}{\rho' \ln b/a} = (\hat{x}\sin\phi' - \hat{y}\cos\phi') \frac{V_i}{\rho' \ln b/a}$$

$$\mathbf{M}^i(\rho') \times \hat{R} = [-\hat{z}\rho' - \hat{\rho}' z] \frac{V_i}{R\rho' \ln b/a}$$

Substituting the above expressions into (4.434.43) yields

$$\begin{aligned} E_z^i(\rho = 0, z) &= \frac{V_i}{\ln b/a} \int_a^b \int_o^{2\pi} \left(jk_o + \frac{1}{R} \right) \frac{e^{-jk_oR}}{4\pi R^2} \rho' d\phi' d\rho' \\ &= \frac{V_i}{2\ln b/a} \int_a^b \left(jk_o + \frac{1}{R} \right) \frac{e^{-jk_oR}}{R^2} \rho' d\rho' \end{aligned} \tag{4.44}$$

Noting that

$$-\frac{d}{d\rho'} \left\{ \frac{e^{-jk_oR}}{R} \right\} = \left(jk_o + \frac{1}{R} \right) \frac{e^{-jk_oR}}{R} \frac{\rho'}{R}$$

(4.444.44) may be written as

$$E_z^i(\rho = 0, z) = -\frac{V_i}{2\ln b/a} \int_a^b \frac{d}{d\rho'} \left\{ \frac{e^{-jk_oR}}{R} \right\} d\rho'$$

to yield

$$E_z^i(\rho = 0, z) = +\frac{V_i}{2\ln b/a} \left[\frac{e^{-jk_o\sqrt{z^2+b^2}}}{\sqrt{z^2+b^2}} - \frac{e^{-jk_o\sqrt{z^2+a^2}}}{\sqrt{z^2+a^2}} \right] \tag{4.45}$$

For simplicity, we may assume

$$E_z^i(\rho = a, z) \approx E_z^i(\rho = 0, z)$$

to be substituted into (4.304.30) and (4.334.33) for the solution of the wire currents. Alternatively, we may pursue a direct evaluation of (4.434.43) to find [?, ?][Tsai, 1972; Thiele, 1973]

$$\begin{aligned} E_z^i(\rho = a, z) = &+V_i \frac{k_o(b^2 - a^2)}{8\ln b/a} \frac{e^{-jk_oR_o}}{R_o^2} \left\{ 2 \left[\frac{1}{k_oR_o} \quad j \left(1 - \frac{b^2 + a^2}{2R_o^2} \right) \right] \right. \\ &\left. + \frac{a^2}{R_o} \left[\left(\frac{1}{k_oR_o} + j - j\frac{b^2 + a^2}{2R_o^2} \right) \left(-jk_o - \frac{2}{R_o} \right) + \left(-\frac{1}{k_oR_o^2} + j\frac{b^2 + a^2}{R_o^3} \right) \right] \right\} \end{aligned} \tag{4.46}$$

where now

$$R_o = \sqrt{z^2 + a^2}$$

with

$$-\ell < z < \ell \,.$$

Figure 4.104.10 illustrates the current on a $1\lambda_o$ dipole computed with a magnetic frill model excitation. The current near the feed is now smoother than that obtained with the delta gap model. However, more samples are required to reach convergence and this is ~~owed to~~ the near singular behavior of the excitation field in (4.454.45).

4.4.3 Plane Wave Incidence

If the cylindrical wire is considered as a scatterer, then $\mathbf{E}^i$ represents the incident field. The simplest form of this is a plane wave given by

$$\mathbf{E}^i = e^{jk_o \mathbf{r}_s \cdot \hat{r}_i} \tag{4.47}$$

where

$$\mathbf{r}_s = a\hat{\rho} + z\hat{z} = a\hat{x} + z\hat{z}|_{\phi=0}$$

if measured on the surface of the wire and

$$\hat{r}_i = \hat{x}\cos\phi_i \sin\theta_i + \hat{y}\sin\phi_i \sin\theta_i + \hat{z}\cos\theta_i \tag{4.48}$$

with (θ_i, ϕ_i) being the usual spherical angles denoting the direction of incidence.

Figs. 4.114.11 and 4.124.12 show the current on the $\lambda_o/2$ and $1\lambda_o$ wire dipoles due to a plane wave incidence excitation. In contrast to the current on a center-fed dipole, this current has no discontinuous derivatives throughout the length of the dipole. Its form on the $\lambda_o/2$ dipole is clearly sinusoidal with its amplitude depending on the incidence angle. The same holds for longer wires with the exception of having a more complex lobing structure which can be explained by invoking the traveling wave theory.

Figure 4.10: Computed current on a center-fed λ_o dipole of radius $a = .005\lambda_o$ via the pulse basis-point matching technique as a function of the sampling density. The source/excitation is the magnetic frill equivalent current as given in (4.454.45).

Figure 4.11: Current on a $\lambda_o/2$ wire of radius $a = .005\lambda$ generated by an incident plane wave at $\theta_i = 90^\circ$ and $\theta_i = 150^\circ$ as computed by the pulse basis-point matching technique ($a = 0.005\lambda_o, N = 101$).

Figure 4.12: Current on a λ_o wire of radius $a = .005\lambda$ generated by an incident plane wave at $\theta_i = 90^\circ$ and $\theta_i = 150^\circ$ as computed by the pulse basis-point matching technique ($a = 0.005\lambda_o, N = 151$).

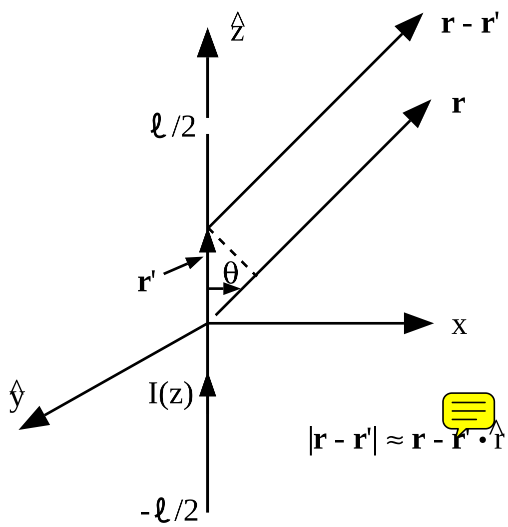

Figure 4.13: Geometry for computing the linear antenna's radiated field.

4.5 Calculation of the Far Zone Field and Antenna Characteristics

Upon solution of the system (4.334.33), one can proceed with the evaluation of the radiation or the scattering patterns if **E** is given by (4.484.48). From (2.772.77) we have

$$
\begin{aligned}
E_\theta^r &\approx jk_o Z_o \sin\theta \int_{-\ell}^{\ell} I(z') \frac{e^{-jk_o|\mathbf{r}-\mathbf{r}'|}}{4\pi|\mathbf{r}-\mathbf{r}'|} dz' \\
&\approx jk_o Z_o \sin\theta \frac{e^{-jk_o r}}{4\pi r} \int_{-\ell}^{\ell} I(z') e^{jk_o z' \cos\theta} dz'
\end{aligned}
\tag{4.49}
$$

Using (14), we get

$$
E_\theta^r(r,\theta) \approx jk_o Z_o \sin\theta \frac{e^{-jk_o r}}{4\pi r} \sum_{n=0}^{N-1} I_n \int_{z_n-\frac{\Delta z}{2}}^{z_n+\frac{\Delta z}{2}} e^{jk_o z' \cos\theta} dz' \tag{4.50}
$$

and upon performing the trivial integration we have

$$\begin{aligned}\mathbf{E}^r(r,\theta) &= jk_oZ_o\frac{e^{-jk_or}}{4\pi r}\Delta z\sin\theta\frac{\sin\left(\frac{k_o\Delta z\cos\theta}{2}\right)}{\left(\frac{k_o\Delta z\cos\theta}{2}\right)}\sum_{n=0}^{N-1}I_ne^{jk_oz_n\cos\theta}\\ &= jk_oZ_o\frac{e^{-jk_or}}{4\pi r}\Delta z\sin\theta\,\mathrm{sinc}\left(k_o\frac{\Delta z}{2}\cos\theta\right)\sum_{n=0}^{N-1}I_ne^{jk_oz_n\cos\theta}\end{aligned} \tag{4.51}$$

The radiation intensity of the antenna is given by

$$\begin{aligned}U(\theta,\phi) &= U(\theta)=\frac{r^2}{2Z_o}\left|E_\theta^r(\theta)\right|^2\\ &= \frac{Z_o}{2}\left(\frac{k_o\Delta z\sin\theta}{4\pi}\right)^2\mathrm{sinc}^2\left(k_o\frac{\Delta z}{2}\cos\theta\right)\left(\sum_{n=1}^{N}I_ne^{jk_oz_n\cos\theta}\right)^2\end{aligned} \tag{4.52}$$

and the radiated power can be computed from

$$P_{\text{rad}}=\int_0^{2\pi}\int_0^{\pi}U(\theta,\phi)\sin\theta\,d\theta\,d\phi=2\pi\int_0^{\pi}U(\theta)\sin\theta\,d\theta \tag{4.53}$$

with the integral to be evaluated numerically.

Given the radiated power, the directivity is found from

$$D=\frac{4\pi U_{\text{max}}}{P_{\text{rad}}}=\frac{4\pi U(\theta=\pi/2)}{P_{\text{rad}}} \tag{4.54}$$

Finally, the gain of the antenna can be easily computed from

$$G(\theta,\phi)=\left.\frac{4\pi U(\theta,\phi)}{P_{\text{in}}}\right|_{\theta=\pi/2}=\frac{Z_o}{2P_{\text{in}}}\frac{(k_o\Delta z)^2}{4\pi}\left(\sum_{n=1}^{N}I_n\right)^2 \tag{4.55}$$

where P_{in} denotes the input power from the generator.

A parameter of crucial importance in controlling the efficiency of the antenna is its input impedance. This is given by

$$Z_{\text{in}}=\frac{V_i}{I_{\text{in}}}=\frac{E_z^i\Delta z}{I_{\text{in}}} \tag{4.56}$$

where $I_{\text{in}} = I_{\frac{N-1}{2}+1}$ is the value of the current element at the terminal under the obvious assumption that N is odd. However, the accuracy of (4.564.56) depends on the accuracy of I_{in} as computed from the solution of the system (4.334.33). Since we discretized the actual current distribution, I_{in} is only an approximation to the input current and is often not of acceptable accuracy unless N is very large. To avoid this difficulty when employing (4.564.56) we may instead use a stationary expression for the input impedance based on power relations. From Poynting's theorem we have

$$\begin{aligned}\frac{1}{2} I_{in} I_{in}^* Z_{in} &= \frac{1}{2} \oiint \mathbf{E}^r \times \mathbf{H}^{r*} \cdot d\mathbf{s} = -\int_{-\ell}^{\ell} \int_0^{2\pi} E_z^r H_\phi^{r*} a \, d\phi \, dz' \\ &= -\frac{1}{2} \int_{-\ell}^{\ell} E_z^r(a, z') I^*(z') dz'\end{aligned} \tag{4.57}$$

Since $\mathbf{J} = \hat{\rho} \times \hat{\phi} H_\phi$ giving $H_\phi = J_z = \frac{I(z)}{2\pi a}$. Thus,

$$Z_{in} = +\frac{1}{|I_{\text{in}}|^2} \int_{-\ell}^{\ell} E_z^i(a, z') I^*(z') dz \tag{4.58}$$

where we have set $E_z^r(a, z) = -E_z^i(a, z)$ as required by the boundary condition on the surface of the wire. Substituting (4.244.24) into (4.584.58) we obtain

$$Z_{in} = \frac{\Delta z}{|I_{\text{in}}|^2} \sum_{n=0}^{N-1} E_z^i(a, z_n) I_n^* \tag{4.59}$$

It is observed, that for a delta gap excitation (see (4.394.39)) (4.594.59) again reduces to (4.564.56). Note also that

$$Re(Z_{in}) = R_{in} = \frac{2P_{\text{rad}}}{|I_{\text{in}}|^2} \, . \tag{4.60}$$

The input impedance as computed from (4.564.56) is shown in Fig. 4.144.14 as a function of the wire's length and for various wire radii. As can be concluded from the presented current computations using the pulse basis-point matching solutions, up to 120 segments per wavelength may be required to accurately sample the current near the feed. When $Im(Z_{in}) = 0$, the dipole is said to be at resonance and its first resonance occurs when 2ℓ is just less than $0.5\lambda_o$, depending on the value of its radius. The bandwidth of an antenna is related to the slope of Z_{in} as a function of frequency and it is seen from Fig. 4.144.14 that thicker dipoles have a larger bandwidth (the thin-wire solution should not be used for $a > \frac{\lambda_o}{50}$ [?][Lin and Richmond, 1975]). Radiation patterns for the $\lambda_o/2$, λ_o and $3\lambda_o/2$ dipoles are given in Fig. 4.154.15. We note, however, that these are identical to those predicted with the assumed sinusoidal distribution which follows from the transmission line model.

When the excitation is a plane wave, we are generally interested in the echo area or radar cross section (RCS) of the wire structure. The RCS is measured in units of length squared and is given by

$$\sigma = \lim_{r\to\infty} 4\pi r^2 \frac{|\mathbf{E}^r|}{|\mathbf{E}^i|^2} \tag{4.61}$$

If the wire length is measured in wavelengths then the units of σ are square wavelengths (λ_o^2) and if the wire length is measured in meters then σ will be given in m^2. The RCS of the $\lambda/2$, λ and 3λ long wires are shown in Figs. 4.164.16 and 4.174.17. The effect of wire thickness on the wire's RCS is predicted in Fig. 4.184.18 where the value of broadside ($\theta_i = 90°$) σ is plotted as a function of the wire's length for three different radii. This is a characteristic curve for the wire scatterer and displays its resonant behavior when $2\ell \approx (n+1)\lambda_o/2$ for odd n. Basically, the RCS of the wire at those lengths reaches a local peak with each successive peak becoming larger as 2ℓ is increased. This property of the wire has been explored in many practical situations and we remark that the location of the RCS peaks should correspond to the wire length at which $Im(Z_{in}) \approx 0$.

We observe that the echo area pattern of the longer wire as given in Fig. 4.174.17 has a very strong lobe near $\theta = \pi$ (near grazing). This is a lobe characteristic to all thin wire scattering patterns and is always the one closest to $\theta = 0°$ or $\theta = \pi$. It is often referred to as the traveling wave lobe and to explain its presence let us assume that the wire is infinite in length. The incident plane wave (4.474.47) will then generate a current of the form $I_1 e^{jk_o z\cos\theta_i}$ where I_1 is a complex constant proportional to the incident wave's strength and can be computed analytically. This is, of course, a traveling current (whose propagation constant matches that of the incident wave) and if the wire is of finite extent, when it reaches the wire ends, it generates additional reflected currents of the form $I_2 e^{jk_o z}$ and $I_3 e^{-jk_o z}$, where I_2 and I_3 are again complex constants. Thus the current on the wire due to a plane wave

Figure 4.14: Input impedance of a dipole as a function of its length 2ℓ for three different wire radii. (a) resistive (b) reactance; The dipole is resonant when the reactance is zero.

Figure 4.15: Radiation power patterns for the $\lambda_o/2$, $1\lambda_o$ and $1.5\lambda_o$ dipoles computed from the numerical solution of the dipole currents ($a = 0.005\lambda_o$).

Figure 4.16: Bistatic radar cross section of three straight wires of length $2\ell = \lambda_o/2$, λ_o and $3\lambda_o$. The wires have a radius of $a = 0.005\lambda_o$ and the incident plane wave is illuminating the wire at an angle of $\theta_i = 150°$ (PWS-basis solution).

Figure 4.17: Backscatter radar cross section ($\theta = \theta_i$) for the three straight wires whose bistatic patterns are given in Fig. 4.16.

excitation can be approximately represented as

$$I(z) = \sum_{n=1}^{3} I_n e^{jk_n z} \tag{4.62}$$

with $k_1 = k_o \cos\theta_o$, $k_2 = +k_o$ and $k_3 = -k_o$. From this representation it is not difficult to observe from the radiation integral (4.494.49) that the scattered field would peak at $\theta = \pi - \theta_i$ and at $\theta = 0$ or π if the coefficients I_n were comparably weighted. However, this is not the case and it turns out that the traveling wave lobe peak occurs when $I_{2,3}$ are at maximum.

The expansion (4.624.62) is, of course, a linear sum of three full wave basis functions, similar to those given by (4.224.22) – (4.234.23). It was constructed on the basis of the physical phenomena that take place on the straight wire and is thus most efficient for computational purposes. However, as noted earlier, this expansion (which may be referred to as a *solution wave* expansion is specific to the straight wire scatterer and cannot be employed for other wire shapes or arbitrary multiple wire structures.

4.6 Piecewise Sinusoidal Basis-Point Matching Solution

The piecewise sinusoidal (PWS) basis expansion renders a continuous current distribution and is thus more representative of the actual solution. This usually translates in less subsections/zones to reach convergence.

Substituting (4.214.21) into (4.184.18) yields

$$I(z) = \sum_{n=0}^{N} I_n \frac{\sin k_o(\Delta z - |z - z_n|)}{\sin k_o \Delta z} \tag{4.63}$$

where $z_n = -\ell + (n+1)\Delta z$. When this is substituted into (4.134.13), we obtain (see Appendix)

$$E_z^i(\rho = a, z) = \frac{+j30}{\sin k_o \Delta z} \sum_{n=0}^{N-1} I_n \left[\frac{e^{-jk_o R_{1n}}}{R_{1n}} \right. \\ \left. -2\cos(k_o \Delta z) \frac{e^{-jk_o R_{2n}}}{R_{2n}} + \frac{e^{-jk_o R_{3n}}}{R_{3n}} \right] \tag{4.64}$$

in which

$$R_{1n} = \sqrt{(z - z_{n-1})^2 + a^2}$$

$$R_{2n} = \sqrt{(z - z_n)^2 + a^2}$$

and

$$R_{3n} = \sqrt{(z - z_{n+1})^2 + a^2}\,.$$

The fact that the radiated field by a sinusoidal source can be evaluated in a closed form is the principal advantage of $S_n(z)$ over $T_n(z)$.

A point matching solution of (4.644.64) follows the same procedure as discussed previously in connection with the pulse basis expansion. Upon evaluation of the coefficients I_n, the radiation pattern is again given by (4.494.49). From (4.634.63) we obtain

$$E_\theta(r,\theta) \approx \frac{jk_oZ_o}{\sin\theta}\frac{e^{-jk_or}}{4\pi r}\sum_{n=0}^{N-1} I_n \int_{z_n-\Delta z}^{z_n+\Delta z} \frac{\sin k_o(\Delta z - |z' - z_n|)}{\sin(k_o\Delta z)} e^{jk_oz'\cos\theta} dz' \tag{4.65}$$

and on carrying out the integration we find

$$E_\theta(r,\theta) \approx j60\frac{e^{-jkr}}{r}\underbrace{\frac{\cos(k_o\Delta z\cos\theta) - \cos(k_o\Delta z)}{\sin\theta\sin(k_o\Delta z)}}_{\text{element pattern}}\sum_{n=0}^{N-1} I_n e^{jk_oz_n\cos\theta} \tag{4.66}$$

The evaluation of other parameters such as radiated power, gain, directivity and input impedance can be performed in a straightforward manner. Not surprisingly, the PWS representation can be shown to yield more accurate results for input impedance computations. This can be attested by examining the wire surface fields generated by the PWS-point matching solution. In contrast to the results in Fig. 4.84.8, it is found that the surface field of this solution is now practically zero without even resorting to the more robust weighted residual method discussed next.

4.7 Method of Weighted Residuals/Moment Method

The point matching technique described above for solving integral equations ensures that the boundary condition is satisfied only at the match points z_m. In general, however, the boundary condition is not necessarily satisfied elsewhere, unless the sampling or testing interval Δz is extremely small and this fact was illustrated in Fig. 4.84.8. This is, of course, not cost effective since the CPU time is proportional to N^3 as given by (4.374.37).

An alternative testing procedure is to satisfy the boundary condition on an average sense over the length of the segment from z_n to z_{n+1}. To express this mathematically, let us first define the interproduct (see for example Harrington [R. F. Harrington(1968)][1968])

$$\langle R(z), W_m(z)\rangle = \int_{-\ell}^{\ell} R(z) W_m^*(z) dz \tag{4.67}$$

and we will hereon refer to $R(z)$ as the residual and $W_m(z)$ as the weighting/test basis functions. Setting

$$R(z) = E_z^i(\rho = a, z) + E_z^r(\rho = a, z)\ , \tag{4.68}$$

choosing

$$W_m(z) = \begin{cases} 1 & z_m - \frac{\Delta z}{2} < z < z_m + \frac{\Delta z}{2} \\ 0 & \text{elsewhere} \end{cases} \tag{4.69}$$

and demanding that

$$\langle R(z), W_m(z)\rangle = 0 \tag{4.70}$$

leads to the integral equation

$$-\int_{z_m-\frac{\Delta z}{2}}^{z_m+\frac{\Delta z}{2}} E_z^i(\rho = a, z) dz = \int_{z_m-\frac{\Delta z}{2}}^{z_m+\frac{\Delta z}{2}} E_z^r(\rho = a, z) dz \tag{4.71}$$

Upon substitution of the expression for E_z^r as extracted from (4.304.30) yields,

$$-\int_{z_m-\frac{\Delta z}{2}}^{z_m+\frac{\Delta z}{2}} E_z^i(\rho = a, z) = -\frac{jZ_o}{2\lambda_o} \sum_{n=0}^{N-1} I_n \int_{z_m-\frac{\Delta z}{2}}^{z_m+\frac{\Delta z}{2}} \left[\Psi_n(z) + \Phi_n(z)\right] dz \tag{4.72}$$

from which we obtain the system

$$[Z_{mn}]\,[I_n] = [V_m] \tag{4.73}$$

where now

$$V_m = -\int_{z_m-\frac{\Delta z}{2}}^{z_m+\frac{\Delta z}{2}} E_z^i(\rho = a, z)dx \tag{4.74}$$

$$Z_{mn} = \frac{-jZ_o}{2\lambda_o}\int_{z_m-\frac{\Delta z}{2}}^{z_m+\frac{\Delta z}{2}} \left[\Psi_n(z) + \Phi_n(z)\right] dz \tag{4.75}$$

These can be evaluated numerically using, for example, Simpson's, midpoint or Gaussian rules of integration [?][Ambramowitz and Stegan, 1964]. Clearly, (4.704.70) along with (4.684.68) and (4.694.69) demand that the boundary conditions be satisfied on an average sense over the wire subintervals. When the weighting functions are piecewise constant (PWC), each current value over the subinterval is given equal weighting in this averaging process. A variety of other choices for $W_m(z)$ have, though, been employed successfully in the past. When $W_m(z)$ are chosen to be the same as the current expansion basis function, the procedure for deriving the resulting system of equations is referred to as Galerkin's method [?, ?][Kantorovich and Krylov, 1959; Jones, 1956]. We also note that when

$$W_m(z) = \delta(z - z_m) \tag{4.76}$$

(4.704.70) reduces to the system (4.304.30) derived by the point-matching technique. The above procedure for discretizing the integral equation is formally referred to as the *weighted residual method* but is most often called the *method of moments* (MoM)[1]. Also, the pulse basis-point matching procedure is more formally referred to as the *collocation method*.

The application of Galerkin's technique has been studied extensively and has been found quite robust for many applications. It is indeed pleasing to know that the method minimizes the residual in the least squares sense. It can be expected that the Galerkin's implementation leads to more robust and efficient computer codes. For example, in the case of a pulse basis expansion,

[1]According to R.F. Harrington, the term "moment methods" was first used by Kantorovitz and Akilov [?][1964].

the Galerkin's solution converges to the correct current using 30% to 50% less segments as shown in Fig. 4.214.21. The solution convergence improves even further if higher order basis functions and used and below we describe the Galerkin's formulation and derive the resulting system of equations for the subsectional sinusoidal basis.

From (4.704.70), with

$$W_m(z) = \begin{cases} \frac{\sin(k_o(\Delta z - |z-z_m|))}{\sin k_o \Delta z} & z_{m-1} < z < z_{m+1} \\ 0 & \text{elsewhere} \end{cases} \tag{4.77}$$

and (see (4.644.64))

$$\begin{aligned} R(z) = E_z^i(\rho = a, z) - \frac{j30}{\sin(k_o\Delta z)} \sum_{n=0}^{N-1} I_n \Bigg[\frac{e^{-jk_oR_{1n}}}{R_{1n}} \\ -2\cos(k_o\Delta z)\frac{e^{-jk_oR_{2n}}}{R_{2n}} + \frac{e^{-jk_oR_{3n}}}{R_{3n}} \Bigg] \end{aligned} \tag{4.78}$$

we obtain the usual system (4.624.62) with

$$V_m = -\int_{z_m-\Delta z}^{z_m+\Delta z} E^i(\rho = a, z) \frac{\sin\left[k_o(\Delta z - |z-z_m|)\right]}{\sin(k_o\Delta z)} dz \tag{4.79}$$

$$\begin{aligned} Z_{mn} = -\frac{j30}{\sin k_o\Delta z} \int_{z_m-\Delta z}^{z_m+\Delta z} \frac{\sin\left[k_o(\Delta z - |z-z_m|\right]}{\sin(k_o\Delta z)} \Bigg[\frac{e^{-jk_oR_{1n}}}{R_{1n}} \\ -2\cos(k_o\Delta z)\frac{e^{-jk_oR_{2n}}}{R_{2n}} + \frac{e^{-jk_oR_{3n}}}{R_{3n}} \Bigg] dz \end{aligned} \tag{4.80}$$

The impedance matrix elements may be easily evaluated numerically as given in (4.804.80) since the integrand is non singular. However, after some manipulation, the integral expression can be simplified and written in terms of the exponential integral which is tabulated [?][Ambramowitz and Stegan, 1964 (p. 228)]. A compact expression for Z_{mn} is [?][?][King, 1957; Richmond and Geary, 1970]

$$Z_{mn} = \frac{+15}{\sin^2(k_o\Delta z)} \sum_{p=-2}^{2} \sum_{q=-1,2} A(p+3) e^{-jk_oq[|z_m-z_n|+p\Delta z]} E(k_o\beta_{pq}) \tag{4.81}$$

where

$$\begin{aligned}
A(1) &= A(5) = 1 \\
A(2) &= A(4) = -4\cos(k_o \Delta z) \\
A(3) &= 2 + 4\cos^2(k_o \Delta z) \\
\beta_{pq} &= \sqrt{a^2 + [|z_m - z_n| + p\Delta z]^2} - q\,[|z_m - z_n| + p\Delta z]
\end{aligned}$$

and $E(\alpha)$ is the exponential integral. It can be defined in terms of the cosine and sine integrals as

$$E(\alpha) = Ci(\alpha) - jSi(\alpha) \tag{4.82}$$

where

$$Ci(\alpha) = -\int_{\alpha}^{\infty} \frac{\cos x}{x} dx \tag{4.83}$$

and

$$Si(x) = \int_0^{\alpha} \frac{\sin x}{x} dx\ . \tag{4.84}$$

A FORTRAN subroutine (one page long) for the numerical evaluation of $E(\alpha)$ is given in Press, etc. [?][1992]. As can be expected, a smaller number of PWS is required to converge to the correct value of the wire current when compared to the pulse basis implementation.

4.8 Moment Method for Non-Linear Wires

Typically, the antenna or scatterer will be composed of curved wire elements. Also, it is possible to model continuous metallic surfaces with a wire grid of sufficient density as shown in the figure. Acceptable grid densities are often 10 or more wires per linear wavelength on the surface.

To develop a Moment Method formulation applicable to curved wires let us consider the curved wire geometry shown below and we may assume for simplicity a constant wire thickness equal to $2a \gg \lambda$. As usual, we are interested

Figure 4.18: Backscatter RCS of three thin wires as a function of length (2ℓ) illuminated by a plane wave at normal incidence ($\theta_i = 90°$). (PWS-point matching solution with $\Delta Z = 0.01\lambda_o$).

Figure 4.19: Convergence of the current distribution on a center-fed dipole of radius $a = 0.005\lambda_o$ with a magnetic frill source. (a) Pulse basis-point matching solution using $N = 81, 101, 181, 221$ and 261 points, (b) Galerkin's pulse basis solution using $N = 101$, 141, 181 and 221 point.

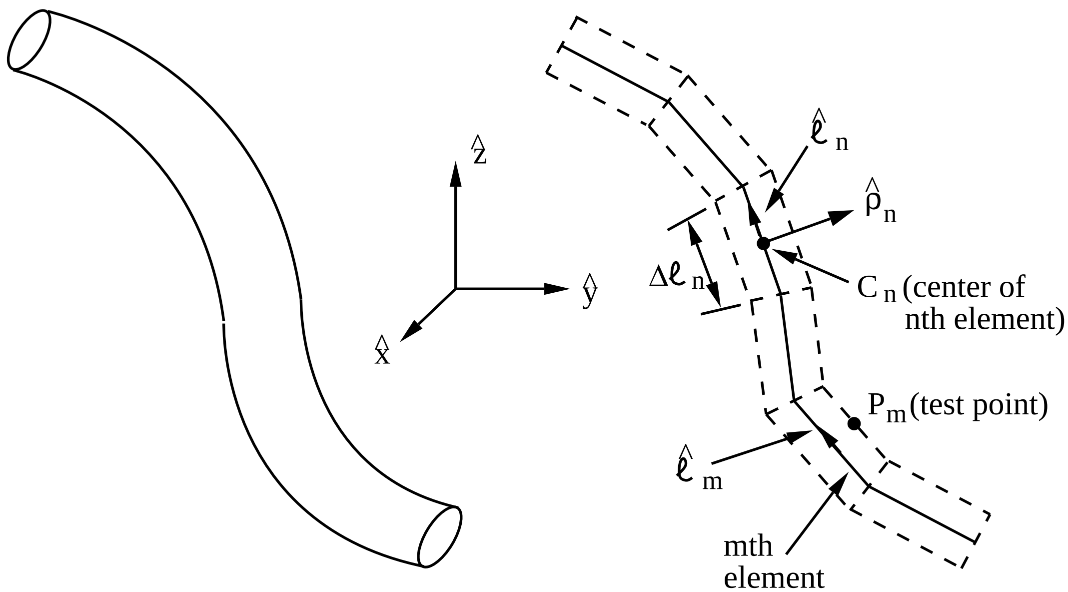

Figure 4.20: Segmentation of a curved wire for numerical modeling.

in determining the wire surface currents or more specifically the equivalent line current through the center of the wire.

In proceeding with a numerical solution, it is first necessary to discretize the wire as shown in Fig. 4.204.20. This amounts to generating a model of the curved wire that is composed of a set of linear segments. Denoting the unit vector along the direction of the mth element as $\hat{\ell}_m$, the boundary condition to be satisfied on its surface is

$$\left(\mathbf{E}^i + \mathbf{E}^r\right) \cdot \hat{\ell}_m = 0 \tag{4.85}$$

If the curved wire is divided into N straight segments, then $\mathbf{E}^r$ can be expressed as

$$\mathbf{E}^r = \sum_{n=1}^{N} \mathbf{E}_n^r = \sum_{n=1}^{N} \hat{\ell}_n \mathbf{E}_{\ell n}^r \tag{4.86}$$

where $\mathbf{E}_n^r$ is the field radiated by each linear segment. When employing PWC basis to expand the current on each element, $\mathbf{E}_n^r$ can be found from (2.522.52) or (3.133.13) upon performing the necessary coordinate transformations. To see this, we begin with the derivation of the fields radiated by a straight

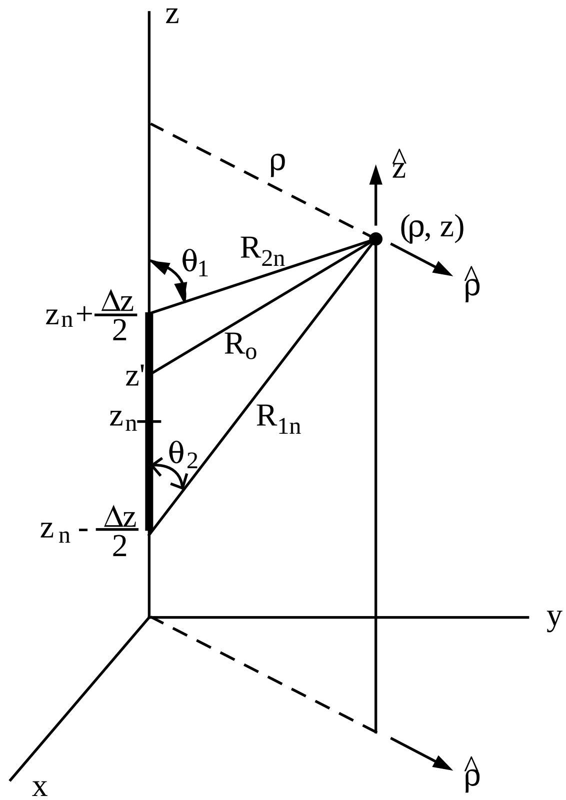

Figure 4.21: Geometry of a monopole situated on the z-axis.

segment (nth segment) carrying a constant current I_n as shown in Fig. 4.214.21. This element is often referred to as a monopulse and we find from (3.133.13) that it radiates the field

$$\mathbf{E}_n^r = \hat{z}E_{nz}^r(\rho, z) + \hat{\rho}E_{np}^r(\rho, z) \tag{4.87}$$

where

$$E_{nz}^r = -\frac{jZ_o}{2\lambda_o}I_n\left[\Psi_n(\rho, z) + \Phi_n(\rho, z)\right] \tag{4.88}$$

and

$$E_{np}^r = j\frac{Z_o k_o}{2\lambda_o}I_n\rho\left[\frac{(1+jk_oR_{1n})}{(k_oR_{1n})^3}e^{-jk_oR_m} - \frac{(1+jk_oR_{2n})}{(k_oR_{2n})^3}e^{-jk_oR_{2n}}\right] \tag{4.89}$$

In these expressions,

$$R_{1n} = \sqrt{\left(z - z_n + \frac{\Delta z}{2}\right)^2 + \rho^2}, \quad R_{2n} = \sqrt{\left(z - z_n - \frac{\Delta z}{2}\right)^2 + \rho^2} \quad (4.90)$$

are simply generalizations of those given in (4.284.28), whereas $\Psi_n(\rho, z)$ and $\Phi_n(\rho, z)$ are the same functions as those defined in (4.314.31) and (4.324.32), respectively, except that

$$R_o = \sqrt{(z - z')^2 + \rho^2}. \quad (4.91)$$

Also, R_{1n} and R_{2n} in (4.314.31) and (4.324.32) must be replaced by the more general expressions (4.904.90).

Given the fields due to the z-directed monopole it is now a straightforward task to derive the corresponding field due to an arbitrarily-oriented monopole. Specifically, for the monopole shown in Fig. 4.224.22 we have that

$$\mathbf{E}_n^r(x, y, z) = \hat{\ell}_n E_{n\ell}^r(x, y, z) + \hat{\rho}_n E_{n\rho}^r(x, y, z) \quad (4.92)$$

where $E_{n\ell}$ and $E_{n\rho}$ are given by (4.884.88) and (4.894.89) with R_o, R_{1n} and R_{2n} redefined as

$$\begin{aligned} R_o &= \sqrt{(x - x_n)^2 + (y - y_n)^2 + (z - z_n)^2} \\ R_{\substack{1n \\ 2n}} &= \sqrt{(x - x_n^{\mp})^2 + (y - y_n^{\mp})^2 + (z - z_n^{\mp})^2} \end{aligned} \quad (4.93)$$

Also, in (4.894.89) ρ must be replaced by $R_{2n} \cos\psi_2 = \mathbf{R}_{2n} \cdot \hat{\ell}_n$.

Having an expression for the field radiated by an arbitrarily oriented wire segment carrying a constant current, we may now proceed with the construction of the system of equations for a pulse basis-point matching solution. On enforcing (4.854.85) at P_m as illustrated in Fig. 4.204.20, for $m = 0, 1, 2, \ldots, N$, we get the usual system (4.334.33). The impedance matrix elements are now given by

$$Z_{mn} = + \left[\left(\hat{\ell}_n \cdot \hat{\ell}_m \right) E_{n\ell}(\tilde{x}_m, \tilde{y}_m, \tilde{z}_m) + \left(\hat{\rho}_n \cdot \hat{\ell}_m \right) E_{n\rho}^r(\tilde{x}_m, \tilde{y}_m, \tilde{z}_m) \right] \quad (4.94)$$

where $\mathbf{r} = \hat{x}\tilde{x}_m + \hat{y}\tilde{y}_m + \hat{z}\tilde{z}_m = (\hat{x}x_m + \hat{y}y_m + \hat{z}z_m) + a\hat{\rho}_m$ with (x_m, y_m, z_m) being the center point of the mth segment and a is its radius. Also,

$$V_m = -\hat{\ell}_m \cdot \mathbf{E}_n^r(\tilde{x}_m, \tilde{y}_m, \tilde{z}_m) \quad (4.95)$$

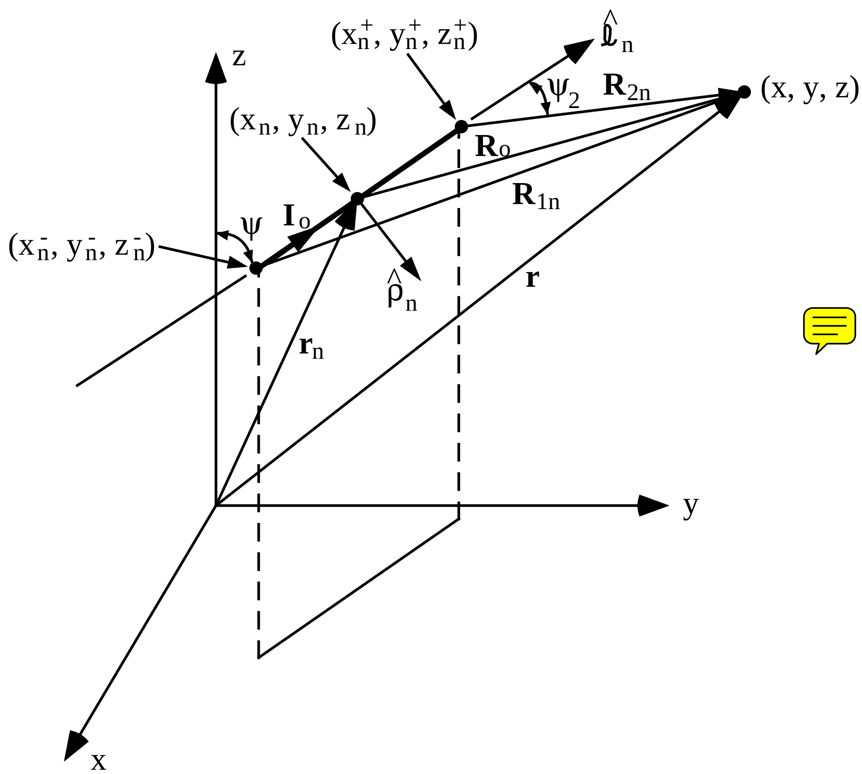

Figure 4.22: Geometry of an arbitrary skewed monopulse.

Figure 4.23: Calculated backscatter echo area of square wire loops at the broadside aspect.

are the elements of the excitation vector. Note that Z_{mn} in (4.944.94) reduces to (4.364.36) for $m = n$.

One of the first implementations of the pulse-basis point matching solution for wire structures was carried out by Richmond [J. H. Richmond(May 1965), ?] [1965, 1966]. In Figs. 4.234.23 and 4.244.24 we present some RCS calculations from Richmond's paper [?][1966] which should serve for validating implementations based on the given pulse basis-point matching solution. Figure 4.234.23 shows the broadside RCS (incident plane wave is impinging along a direction normal to the plane containing the wire loop) of a square loop as a function of L/λ, where L^2 denotes the area enclosed by the loop. Of importance is the observation that solid structures can be modeled by a grid of wires. For example, the square metallic plate shown in figure 4.24 was modeled by a grid of 8 vertical and 8 horizontal wires with the wire radii set equal to $L/100$, where L is the side length of the plate. For an accurate simulation of solid surfaces, Lin and Richmond [?][1975] recommend that the wire separation be no greater than $\lambda_o/4$ and the wire radius be chosen to be about 1/25 of this separation distance. Others have used wire grid modeling (see fig. 4.26) to evaluate the radiation performance of reflector antennas [?][Poggio and Miller,1973] wire antennas on aircraft [?][Diaz, 1970], or on some solid metallic structure [?, ?][Thiele, 1973; Trueman et al, 1991].

To construct the moment method equations for a non-linear wire using the Galerkin's procedure with PWS basis, we must first obtain the radiated fields due to an arbitrarily oriented dipole. Referring to Fig. 4.274.27 and generalizing the results stated in a problem of this chapter, we obtain that

$$\mathbf{E}_n^r(x,y,z) = \hat{\ell}_n E_{n\ell}^r(x,y,z) + \hat{\rho}_n E_{n\rho}^r(x,y,z) \tag{4.96}$$

where

$$E_{n\ell}^r(x,y,z) = -\frac{j30}{\sin k_o\Delta\ell} I_n \left[\frac{e^{-jk_oR_{1n}}}{R_{1n}} - 2\cos(k_o\Delta\ell)\frac{e^{-jk_oR_{2n}}}{R_{2n}} + \frac{e^{-jk_oR_{3n}}}{R_{3n}}\right] \tag{4.97}$$

and

$$\begin{aligned} E_{n\rho}^r(x,y,z) &= \frac{j30}{R_{2n}\sin\psi_{2n}\sin(k_o\Delta\ell)} I_n \left[\cos\psi_{1n}e^{-jk_oR_{1n}}\right. \\ &\quad \left. - 2\cos(k_o\Delta\ell)\cos\psi_{2n}e^{-jk_oR_{2n}} + \cos\psi_{3n}e^{-jk_oR_{3n}}\right] \end{aligned} \tag{4.98}$$

In these, I_n denotes the value of the current at (x_n, y_n, z_n),

$$\begin{aligned} R_{1n} &= \sqrt{(x-x_{n-1})^2 + (y-y_{n-1})^2 + (z-z_{n-1})^2} \\ R_{2n} &= \sqrt{(x-x_n)^2 + (y-y_n)^2 + (z-z_n)^2} \\ R_{3n} &= \sqrt{(x-x_{n+1})^2 + (y-y_{n+1})^2 + (z-z_{n+1})^2} \end{aligned} \tag{4.99}$$

have the same geometrical definitions as those given earlier in section 4.6, and $\cos\psi_{in} = (\hat{\ell}_n \cdot \mathbf{R}_{in})/R_{in}$, for $i = 1, 2, 3$, as illustrated in Fig. 4.274.27.

Figure 4.24: Echo area of perfectly conducting square plates at the broadside aspect (wire diameter $d = L/50$). After Richmond [?][IEEE AP-T, 1966].

Figure 4.25: Backscatter echo area of perfectly conducting spheres. (The wire grid was generated by rotating a 20 sides regular polygon. The number of polygons was $\frac{70R}{\lambda}$, where R is the sphere radius. The wire radius was set to $a = 0.005\lambda$.) After Richmond [?][IEEE AP-T, 1966].

Figure 4.26: Illustration of wire grid models of solid surfaces.

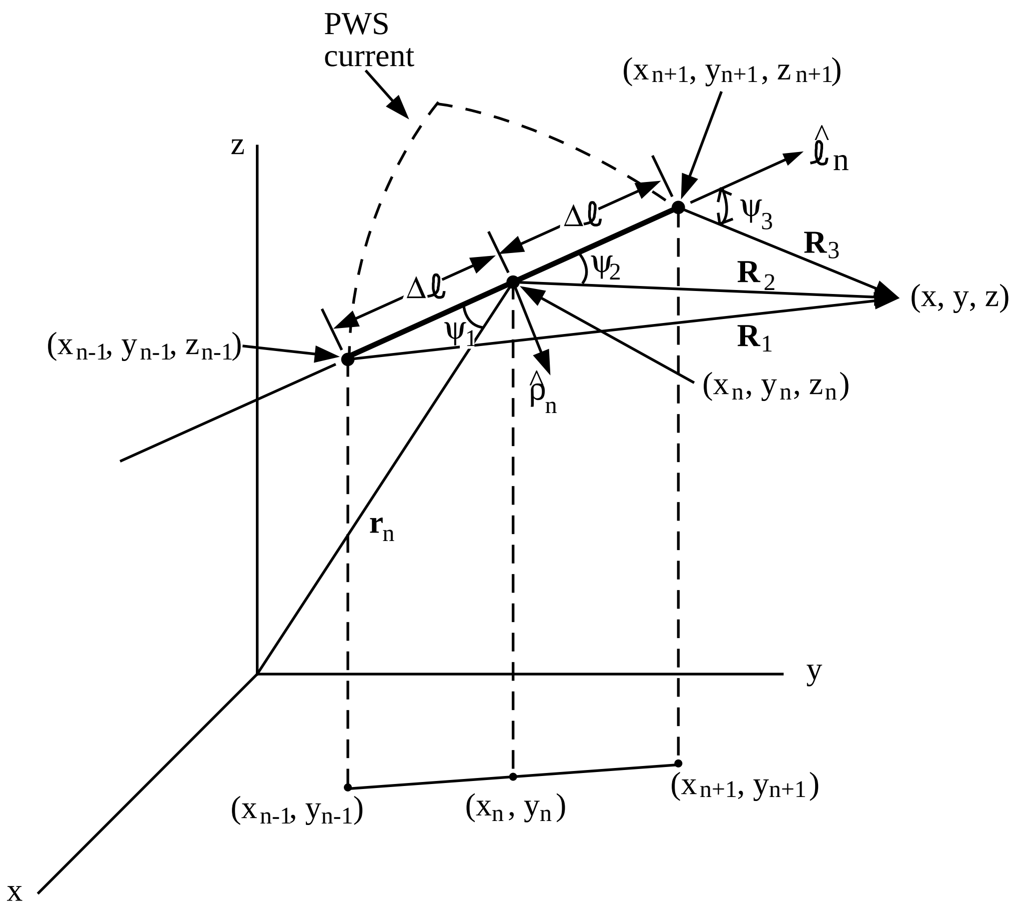

Figure 4.27: Geometry of an arbitrarily oriented dipole.

We are now ready to proceed with the application of Galerkin's method to construct the system of N equations. The equations are constructed from $(m = 0, 1, 2, \ldots, N-1)$

$$\sum_{n=0}^{N-1} I_n \int_{C_m} \mathbf{E}_n^r(x,y,z) \cdot \hat{\ell}_m W(\ell) d\ell = -\int_{C_m} \mathbf{E}^i \cdot \hat{\ell}_m W(\ell) d\ell \qquad (4.100)$$

where the weighting function is now given by

$$W(\ell) = \frac{\sin[k_o(\Delta\ell - |\ell|)]}{\sin(k_o \Delta\ell)} \qquad |\ell| < \Delta\ell \qquad (4.101)$$

and the contour C_m specifies integration over the mth straight segment of the curved wire(s). When (4.1004.100) is put in the usual matrix form (4.334.33), the associated impedance matrix elements are therefore given by

$$Z_{mn} = \int_{C_m} \mathbf{E}_n^r(x,y,z) \cdot \hat{\ell}_m W(\ell) d\ell \qquad (4.102)$$

and to perform the implied integration, it is necessary to replace (x, y, z) with their appropriate parametric representations. Since (4.1004.100) is enforced on the wire surface, it follows that the appropriate parametric representations are

$$\begin{aligned} x &= x_m + a(\hat{\rho}_m \cdot \hat{x}) + \ell(\hat{\ell}_m \cdot \hat{x}) \\ y &= y_m + a(\hat{\rho}_m \cdot \hat{y}) + \ell(\hat{\ell}_m \cdot \hat{y}) \\ \hat{z} &= z_m + a(\hat{\rho}_m \cdot \hat{z}) + \ell(\hat{\ell}_m \cdot \hat{z}) \end{aligned} \qquad (4.103)$$

and the integration is then carried out from $-\Delta\ell$ to $\Delta\ell$. As expected, when $m = n$, Z_{mn} in (4.1024.102) reduces to (4.804.80).

A general purpose computer program based on the PWS Galerkin's method has been written by Richmond [?][1974]. This program was used [?][Lin and Richmond, 1975] to construct wire grid models and aircraft for RCS analysis (see Fig. 4.264.26). As can be realized, because of the importance of wire antennas and their earlier utility for modeling solid structures, the interested reader will find that the literature is very rich on different formulations for wire analyses (see for example Miller and Deadrick [?][1975] for a survey).

Also, general purpose computer programs are readily available. Perhaps the most widely used program is the Numerical Electromagnetics Code (NEC) developed by Poggio and Burke [?][1981] at Lawrence Livermore Laboratories. The basis functions employed in this program are [?][Yeh and Mei (1967)]

$$f_n(z) = A_n + B_n \sin[k_o(z - z_n)] + C_n \cos[k_o(z - z_n)] \tag{4.104}$$

for $|z - z_n| < \frac{\Delta z}{2}$, where z_n denotes the center of the wire segment and A_n, B_n, C_n are constants to be determined. Two of these constants are eliminated by simply enforcing current continuity at the two ends of the nth segment or via application of Kirchhoff's current law (charge conservation) at wire junctions (the other constant is determined by solving the system resulting from point matching). This is necessary, since the above basis functions do not guarantee continuity across the wire junctions as is the case with the overlapping PWS and Piecewise linear expansions. If a wire segment has one of its ends "free" (i.e. not connected to any other segment), the NEC code enforces the condition

$$|I(z)|_{\substack{at\\end}} = \mp \frac{1}{k_o} \frac{J_1(k_o a)}{J_o(k_o a)} \left. \frac{dI(z)}{dz} \right|_{\substack{at\\end}} \tag{4.105}$$

where $J_{0,1}(k_o a)$ denote the Bessel functions of order 0 and 1, and the + sign is selected if the current is flowing toward the segment's termination. This condition accounts for current leakage onto the end of the finite thickness wire.

4.9 Wires of Finite Conductivity

When the wire (or a portion of it) is of finite conductivity, the boundary condition to be satisfied is

$$\mathbf{J}_v = \sigma \mathbf{E}^{tot} \tag{4.106}$$

where $\mathbf{E}^{tot}$ is the total field within the wire, $\mathbf{J}_v$ is the volume current in A/m^2 and σ denotes the wire conductivity. For $a \ll \ell$ we can again replace $\mathbf{J}_v$ by an equivalent filamentary current at the center of the wire given by

$$I = \pi a^2 J_v \tag{4.107}$$

Incorporating this into (4.1064.106) yields the condition

$$\mathbf{E}^{tot} = \hat{\ell} R_w I(\ell) \quad \text{ or } \quad E^i_\ell + E^r_\ell = R_w I(\ell) \tag{4.108}$$

where

$$R_w = \frac{1}{\pi a^2 \sigma} \tag{4.109}$$

can be referred to as the resistivity of the wire.

The boundary condition (4.1084.108) must now replace the one given in (4.14.1). This amounts to a modification of the impedance elements from Z_{mn} to Z'_{mn}, where

$$Z'_{mn} = \begin{cases} Z_{mn} & n \neq m \\ -R_w(\ell_m) \int_{\Delta \ell_m} f_m(\ell) W_m(\ell) d\ell + Z_{mm} & n = m \end{cases} \tag{4.110}$$

in which $R_w(\ell_m)$ denotes the resistivity of the wire at the mth element and $\mathbf{E}_n^r$ is the field radiated by the nth element. The wire current is expanded in the usual manner to yield the system

$$[Z'_{mn}]\{I_n\} = \{V_m\} \tag{4.111}$$

for a solution of the element amplitude coefficients I_n.

Often the wire antenna or scatterer with distributed loads is characterized with a surface impedance Z_s. The boundary condition satisfied on the surface of the wire then is

$$\mathbf{E}^{tot} = Z_s \mathbf{J}_s \tag{4.112}$$

where $\mathbf{J}_s$ denotes the surface current. Since

$$\mathbf{J}_s = \hat{\ell} \frac{I(\ell)}{2\pi a} \tag{4.113}$$

(4.1124.112) may be rewritten as

$$\mathbf{E}^{tot} = \hat{\ell} \frac{Z_s}{2\pi a} I(\ell) \tag{4.114}$$

This is similar to (4.1084.108) and thus a solution for the wire currents is found by setting the impedance elements equal to

$$Z'_{mn} = -\frac{Z_s}{2\pi a} \int_{\Delta \ell_m} f_n(\ell) W_m(\ell) d\ell + Z_{mn} \tag{4.115}$$

where Z_{mn} are the corresponding elements for the perfectly conducting wire. The integral in (4.1154.115) is only over the common domain of the weighting and expansion functions. Thus, if $W_m(\ell)$ and $f_n(\ell)$ are among those in (4.194.19) – (4.214.21) Z'_{mn} will be equal to Z_{mn} except for the matrix elements $Z_{m(m\pm1)}$ and $Z_{(m\pm1)m}$.

4.10 Construction of Integral Equations via the Reaction/Reciprocity Theorem

The integral equations derived earlier via the application of the Moment Method procedure can also be derived by invoking the reaction or reciprocity theorem discussed in chapter 1. The reaction theorem is a mathematical relationship between two sets of sources and their generated fields. Assuming $(\mathbf{J}, \mathbf{M})$ generate the fields $(\mathbf{E}, \mathbf{H})$ and that $(\mathbf{J}_t, \mathbf{M}_t)$ generate the fields $(\mathbf{E}_t, \mathbf{H}_t)$, the reaction theorem states

$$\int\int\int (\mathbf{E} \cdot \mathbf{J}_t - \mathbf{H} \cdot \mathbf{M}_t)\, dv = \int\int\int (\mathbf{E}_t \cdot \mathbf{J} - \mathbf{H}_t \cdot \mathbf{M})\, dv\ . \tag{4.116}$$

Let us now set

$$(\mathbf{E}, \mathbf{H}) = \left(\mathbf{E}^r + \mathbf{E}^i, \mathbf{H}^r + \mathbf{H}^i\right)$$

where $(\mathbf{E}^r, \mathbf{H}^r)$ are the fields radiated by the wire current J_s in the presence of the incident field $(\mathbf{E}^i, \mathbf{H}^i)$ having their source at infinity. Expression (4.1164.116) then becomes

$$\int\int\int (\mathbf{E}^r \cdot \mathbf{J}_t - \mathbf{H}^r \cdot \mathbf{M}_t)\, dv + \int\int\int \left(\mathbf{E}^i \cdot \mathbf{J}_t - \mathbf{H}^i \cdot \mathbf{M}_t\right) dv$$
$$= \oint\!\!\oint (\mathbf{E}_t \cdot \mathbf{J}_s - \mathbf{H}_t \cdot \mathbf{M}_s)\, ds \tag{4.117}$$

We now choose $\mathbf{M}_t = 0$ and set

$$\mathbf{J}_t = \hat{\ell}_m W_m(\ell) = \mathbf{J}_m(\ell) \tag{4.118}$$

concentrated at the center of the nth element of the perfectly conductive wire, where $W_m(\ell)$ is usually chosen to be equal (Galerkin's method) to the equivalent line current of the wire's mth element. The field generated by this source is now zero (essentially $\mathbf{J}_t$ radiates inside a closed hollow conductor) and (4.1174.117) further reduces to

$$\oint\!\!\oint_{\substack{\text{wire}\\ \text{surface}}} \mathbf{E}^r \cdot \mathbf{J}_m ds = -\oint\!\!\oint_{\substack{\text{wire}\\ \text{surface}}} \mathbf{E}^i \cdot \mathbf{J}_m ds \tag{4.119}$$

when $\mathbf{J}_m$ is replaced by its equivalent line current at the center of the wire we have

$$\int\int \mathbf{E}^r \cdot \hat{\ell}_m W_m(\ell) d\ell = -\int\int \mathbf{E}^i \cdot \hat{\ell}_m W_m(\ell) d\ell \tag{4.120}$$

which is the same as (4.774.77) derived by the method of weighted residuals.

4.11 Iterative Solution Methods: The Conjugate Gradient Method

Instead of inverting the impedance matrix $[Z_{mn}]$ for a solution of the system (4.334.33) or (4.734.73), one could employ an iterative solution scheme. Among the numerous iterative solution schemes for such a system, the conjugate gradient (CG) method is most attractive because it guarantees convergence in a maximum of N iterations for an N-dimensional system (ignoring round-off errors). The CG method is a non-linear, semi-direct iterative scheme and was introduced by Hesteness and Steifel [**?**][1952] independently more than 40 years ago. Beginning with a random initial guess of the solution (including the zero vector) vector $\{I_n\}$, convergence is accomplished via a systematic orthogonalization of the solution vector with respect to the residual vector defined as the difference between the left and right hand sides of the system. The residual vector is computed at the end of each iteration and is used to find the next correction to the solution vector. The correction vectors are chosen to be orthogonal to the residual vectors which are linearly independent. This is an essential condition for guaranteeing the convergence of the algorithm since at the Nth iteration the solution vector would have been constructed by N independent vectors (conjugate directions) which form a basis set of the N-dimensional space. Moreover, the algorithm will first proceed with corrections which will most greatly impact the minimization of the next residual vector. Consequently, convergence to within a reasonable degree of accuracy can be achieved after only a few (normally less than $N/3$) iterations.

The CG algorithm is derived in the Appendix and for the pertinent system it proceeds as follows:

Initialize the residual vector and conjugate direction:

$$
\begin{aligned}
\{r_1\} &= \{V\} - [Z]\{I^1\} \\
\beta_o &= \frac{1}{|[Z]^a\{r_1\}|^2} \\
p_1 &= \beta_o[Z]^a\{r_1\}
\end{aligned}
$$

For $k = 1, \ldots, n$ DO

$$
\begin{aligned}
\alpha_k &= \frac{1}{|[Z]\{p_k\}|^2} \\
\{I^{k+1}\} &= \{I^k\} + \alpha_k\{p_k\} \\
\{r_{k+1}\} &= \{r_k\} - \alpha_k[Z]\{p_k\} \\
\beta_k &= \frac{1}{|[Z]^a\{r_{k+1}\}|^2} \\
\{p_{k+1}\} &= \{p_k\} + \beta_k[Z]^a\{r_{k+1}\}
\end{aligned}
$$

terminate loop when normalized residual error

$$
\frac{|r_{k+1}|}{|[Z]^a\{V\}|} < \text{ tolerance}
$$

or when $k = N$.

In the above algorithm, the columns or vectors $\{I^k\}$ represent the current expansion coefficients after the $(k-1)$th iteration, $\{r_k\}$ are the residual vectors and $\{p_k\}$ are the conjugate directions discussed above. Also, $[Z]^a$ denotes the adjoint of the impedance matrix which is equal to the complex conjugate transpose of $[Z_{mn}]$ and

$$
|I^k|^2 = \sum_{n-1}^{N} I_n^k (I_n^k)^* \tag{4.121}
$$

is the square norm of the vector $\{I^k\}$. Typical values for the tolerance range from .01 to 10^{-4}.

Excluding initialization, the above CG algorithm requires $2N^2 + 5N + 2$ multiplications and divisions (i.e. operations) per iteration. Thus, the CPU time required to reach convergence is of order $N^2 N_I$, if N_I is the number of iterations required to satisfy the tolerance condition. Thus, if N_I is not a small faction of N, the required CPU time to solve the system will again be of order N^3. However, the major advantage of the CG method is realized when the $[Z]$ matrix is Toeplitz as is the case for the straight wire. In this case, the fast Fourier transform (FFT) can be combined with the CG method to reduce the storage requirements and speed-up the solution. To see how this is accomplished let us first return to the original integral equation (4.114.11). By invoking the one-dimensional Fourier transform pair defined in (2.1712.171) and the convolution theorem we can rewrite (4.114.11) as

$$\left\{E_z^i(\rho = a, z)\right\} = \frac{jZ_o}{k_o}\mathcal{F}^{-1}\left\{\widetilde{I}(k_z)(k_o^2 - k_z^2)\widetilde{G}_{wr}(k_z)\right\} \tag{4.122}$$

where

$$\widetilde{I}(k_z) = \mathcal{F}\{I(z)\} = \int_{-\infty}^{\infty} I(z)P_{2\ell}(z)e^{-jk_z z}dz = \int_{-\ell}^{\ell} I(z)e^{-jk_z z}dz \tag{4.123}$$

and $\widetilde{G}_{wr}(k_z)$ is correspondingly the Fourier transform of $G_{wr}(z)$ defined in (4.104.10). It is given by

$$\widetilde{G}_{wr}(k_z) = \int_{-\infty}^{\infty} \frac{e^{-jk_o\sqrt{z^2+a^2}}}{4\pi\sqrt{z^2+a^2}}dz = \frac{1}{2\pi}K_o(a\sqrt{k_z^2 - k_o^2}) \tag{4.124}$$

where K_o is the modified Bessel function of the second kind and from (2.1702.170) $\sqrt{k_o^2 - k_z^2} = -j\sqrt{k_z^2 - k_o^2}$. If we were to use the integral equation (4.74.7) which involves the unreduced wire kernel then $\widetilde{G}_{wr}(k_z)$ need be replaced by the transform of $G_{wu}(z)$ given by

$$\widetilde{G}_{wu}(k_z) = \frac{1}{2\pi}I_o(a\sqrt{k_z^2 - k_o^2})K_o(a\sqrt{k_z^2 - k_o^2}) \tag{4.125}$$

in which I_o is the modified Bessel function of the first kind. Note that although K_o in (4.1244.124) and (4.1254.125) becomes infinite when $k_o = k_z$, the argument of the inverse transform operator in (4.1224.122) vanishes at that point because of the multiplying factor $(k_o^2 - k_z^2)$.

The importance of the algebraic expression (4.1224.122) is apparent when it is realized that its right hand side gives the value of the entire column (i.e. for all z_m) resulting from the operation $[Z]\{I\}$ without having to actually generate and store the square matrix $[Z]$ or perform the matrix multiplication. However, before we can make practical use of this advantage, it is necessary to rewrite (4.1224.122) in terms of the discrete Fourier transform (DFT) to permit its implementation on a computer. As a first step toward this, we define the discrete transform pair

$$\hat{I}_p = \hat{I}(p\Delta k_z) = \sum_{n=0}^{N-1} I(n\Delta z)W^{np} \tag{4.126a}$$

$$I_n = I(n\Delta z) = \frac{1}{N}\sum_{p=0}^{N-1} \hat{I}^*(p\Delta k_z)(W^{np})^* \tag{4.126b}$$

where $W = e^{-2\pi/N}$, Δk_z is the subinterval in the spectral domain given by $\Delta k_z = 1/N\Delta z$ and $\hat{I}_p = \hat{I}(p\Delta f)$ is the discrete transform of the sequence I_n.

Upon rewriting the expansion (4.184.18) as

$$I(z) = \sum_{n=0}^{N-1} I_n f_n(z - z_n) = f(z) * \sum_{n=0}^{N-1} I_n \delta(z - z_n) \tag{4.127}$$

where the * indicates convolution and taking its Fourier transform it is seen that the discrete form of $\widetilde{I}(k_z)$ is given by

$$\widetilde{I}(k_z) = \tilde{f}(k_z)\hat{I}_n \tag{4.128}$$

provided we set $k_z = n\Delta k_z$ for calculating $\tilde{f}(k_z)$. If pulse (PWC) basis are employed as expansion functions then

$$\tilde{f}(k_z) = \widetilde{P}_{\Delta z}(k_z) = \Delta z\frac{\sin(k_z\Delta z/2)}{k_z\Delta z/2} = \Delta z \text{ sinc } (k_z\Delta z/2) \tag{4.129}$$

and for PWS basis,

$$\tilde{f}(k_z) = \widetilde{S}(k_z) = \frac{2k_o[\cos(k_z\Delta z) - \cos(k_o\Delta z)]}{(k_o^2 - k_z^2)\sin(k_o\Delta z)} \tag{4.130}$$

We note that as $\Delta z \to 0$ then (4.1294.129) and (4.1304.130) reduce to a value equal to Δz and thus

$$\widetilde{I}(k_z) \approx \Delta z \hat{I}_n$$

which is an expected result implying the basis $f(z) = \Delta z \delta(z)$.

The result (4.1284.128) can now be substituted into (4.1224.122) and perform the required DFT by setting $k_z = n\Delta k_z = n/N\Delta z$. However before doing so, it is instructive to also replace the transform of the derivative $\frac{\partial}{\partial z}$ by its discrete counterpart. To obtain it, we observe that

$$\mathcal{F}\left\{\frac{\Delta G(z)}{\Delta z}\right\} = \mathcal{F}\left\{\frac{G\left(z+\frac{\Delta z}{2}\right) - G\left(z-\frac{\Delta z}{2}\right)}{\Delta z}\right\} = j\frac{2\sin\left(k_z\frac{\Delta z}{2}\right)}{\Delta z}\widetilde{G}(k_z) \tag{4.131}$$

which is the transform of the discrete derivative based on the two point formula. It simply implies that in (4.1224.122) we must make the replacement

$$k_z \to \frac{2\sin\left(k_z\frac{\Delta z}{2}\right)}{\Delta z} = k_z \text{ sinc } \left(k_z\frac{\Delta z}{2}\right)$$

where sinc $\left(k_z\frac{\Delta z}{2}\right) \to 1$ as $\Delta z \to 0$, an expected result. Finally, to obtain the discrete counterpart of $\widetilde{G}_{wr}(k_z)$ the simplest approach is to replace it by the sample train $\widetilde{G}_{wr}(p\Delta k_z)$ with $p = -(N-1), \ldots, 0, 1, \ldots, N$ since the DFT must be of finite length equal to $2N$ in order to satisfy the convolution requirements. However, unless $\widetilde{G}_{wr}(k_z)$ is of negligible value for $|k_z| > N\Delta k_z = 1/\Delta z$, this truncation will cause aliasing errors which will affect the convergence of the CG algorithm and the accuracy of the solution. To avoid aliasing, one approach is to increase the size of the DFT. Generally, though, the DFT must be an integer power of 2 to take advantage of the available FFT algorithms. If we then set $M = 2^\gamma$, where $M > 2N-1$, in accordance with the above discussion we must have

$$\gamma = \text{Integer } \{\log_2(2N-1) + \rho\} \tag{4.132}$$

where $\rho \geq 1$ is an integer and determines the order of the FFT's dimension or pad. The minimum value of ρ is unity and can be increased as required to reduce aliasing. In this case all arrays must be increased accordingly, and except for $\widetilde{G}_{wr}(n\Delta k_z)$ the rest must be padded with zeros. In particular, the first N points of the array $\{I_n\}$ are filled with the initial guess and the array is then transformed using a length of $M = 2^\gamma$ to obtain $\{\hat{I}_n\}$. To recover the next $\{I_n\}$ after inverse transformation only the first N points are again kept and the others are zeroed.

In accordance with the above discussion, the discrete counterpart of (4.1054.105) is

$$\{V_m\} = -\frac{jZ_o}{k_o} DFT^{-1}\left\{\left[k_o^2 - n^2(\Delta k_z)^2 \,\mathrm{sinc}^{\,2}\left(\frac{n\Delta k_z}{2}\Delta z\right)\right]\hat{I}_n \tilde{f}(n\Delta k_z)\widetilde{G}_{wr}(n\Delta k_z)\right\} \tag{4.133}$$

The left and right hand sides of this equality should be interpreted as columns or vectors of length N with the one from the right side obtained after truncating the padded array. More specifically $V_m = -E_z^i(\rho = a, z_m)$ whereas the right side should be equal to the column generated from the operation $[Z]\{I_n\}$. Thus, in the CG algorithm we should set

$$[Z]\{I_n\} = -\frac{jZ_o}{k_o} DFT^{-1}\left\{ \left[k_o^2 - n^2(\Delta k_z)^2 \,\mathrm{sinc}^{\,2}\left(\frac{n\Delta k_z \Delta z}{2}\right)\right] \cdot \hat{I}_n \tilde{f}(n\Delta k_z)\widetilde{G}_{wr}(n\Delta k_z)\right\} \tag{4.134}$$

This eliminates a need to generate the matrix thus reducing the storage to $O(N)$ instead of $O(M^2)$ required with the direct solution. Moreover, because the DFT can be computed by performing only $M\log_2 M$ operations (provided $M = 2^\gamma$), the required CPU time per iteration is reduced to $4M(1+\log_2 M)$. Thus, the total solution CPU time becomes $4MN_I(1+\log_2 M)$ and as before N_I denotes the number of iterations to reach convergence. Actual CPU times for computing the current of a $1\lambda_o$ dipole are given in Fig. 4.214.21. As seen, the CPU time in conjunction with the FFT (usually referred to as the CGFFT method) is nearly a linear function of the number of unknowns whereas the CPU time associated with the direct (matrix inversion) solution is a quadratic function of the unknowns. Also, we observe from Fig. 4.264.26 that the use of higher order basis leads to better convergence rates.

We close this section by noting that an alternative and more appropriate way to compute the column $[Z]\{I_n\}$ is to consider the discretized equation

$$V_m = \sum_{n=0}^{N-1} I_n Z_{mn} = \sum_{n=0}^{N-1} I_n Z(m-n) = \sum_{n=0}^{N-1} I_n Z_{m-n}$$

Figure 4.28: A comparison of the CPU time required by the MOM and the CGFFT formulations for the solution of the $1\lambda_o$ wire dipole problem.

Then by application of the discrete convolution theorem it follows that

$$\{V_m\} = DFT^{-1}\{\hat{Z}\hat{I}_n\}$$

where $\hat{Z}$ denotes the discrete transform of the sequence Z_{0n} or the sequence $Z_{m-n} = Z_p$ with $p = -(N-1), \ldots, 0, 1, 2, \ldots, N-1$. Because of the periodicity of the discrete FFT aliasing is eliminated once the FFT length is set equal to $2N-1$ to accommodate spreading due to the convolution. The sequence Z_{0n} can be obtained from the expressions given earlier by (4.364.36), (4.754.75) or (4.804.80). If $2N-1$ is not a power of 2 then the values of the Z_p sequence should be arranged as shown in Fig. 4.274.27.

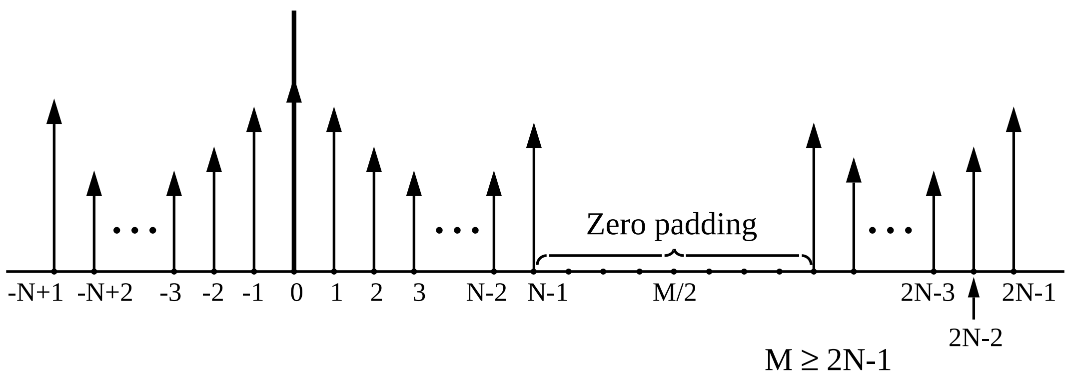

Figure 4.29: Arrangement of the $Z_{m-n} = Z_p$ sequence before inverse fourier transformation.

In general the computation of the Z_{mn} elements may be difficult due to kernel singularities and the requirement to perform rather involved integrations. In this case, a third alternative would be to return to (4.1344.134) and replace $\widetilde{G}_{wr}(k_z)$ by the discrete transform of the sequence

$$G_{wr}(z_n) = \frac{e^{-jk_o\sqrt{(n\Delta z)^2+a^2}}}{4\pi\sqrt{(n\Delta z)^2+a^2}}$$

with $n = -N-1, \ldots, 0, 1, \ldots, N-1$. This procedure should substantially reduce aliasing errors and is equivalent to setting

$$\hat{Z}_n = -\frac{jZ_o}{k_o}\left\{\left[k^2 - n^2(\Delta k_z)^2 \text{ sinc } \left(\frac{n\Delta k_z \Delta z}{2}\right)\right]\tilde{f}(n\Delta k_z)\hat{G}_{wr}\right\}. \quad (4.135)$$

where $\hat{G}_{wr}$ corresponds to the transform of the discrete sequence $G_{wr}(z_n)$. By taking the inverse DFT of the above $\hat{Z}_n$ we will then (approximately) recover the original sequence Z_n. Any aliasing errors will be due to the truncation of $\tilde{f}(k_z)$ but these should be negligible.